HYDROLOGICAL PROCESSES
*Hydrol. Process.* **18**, 505–530 (2004)
Published online in Wiley InterScience (www.interscience.wiley.com). DOI: 10.1002/hyp.1335

# Stormflow generation in a small rainforest catchment in the Luquillo Experimental Forest, Puerto Rico

J. Schellekens,[1,2]* F. N. Scatena,[3] L. A. Bruijnzeel,[1] A. I. J. M. van Dijk,[1]
M. M. A. Groen[1] and R. J. P. van Hogezand[1]

[1] *Faculty of Earth and Life Sciences, Vrije Universiteit Amsterdam, De Boelelaan 1085, 1081 HV Amsterdam, The Netherlands*
[2] *WL | Delft Hydraulics, Rotterdamseweg 185, 2629 HD Delft The Netherlands*
[3] *United States Department of Agriculture, Forest Service, International Institute of Tropical Forestry, Rio Piedras, Puerto Rico*

## Abstract:

Various complementary techniques were used to investigate the stormflow generating processes in a small headwater catchment in northeastern Puerto Rico. Over 100 samples were taken of soil matrix water, macropore flow, streamflow and precipitation, mainly during two storms of contrasting magnitude, for the analysis of calcium, magnesium, silicon, potassium, sodium and chloride. These were combined with hydrometric information on streamflow, return flow, precipitation, throughfall and soil moisture to distinguish water following different flow paths. Geo-electric sounding was used to survey the subsurface structure of the catchment, revealing a weathering front that coincided with the elevation of the stream channel instead of running parallel to surface topography. The hydrometric data were used in combination with soil physical data, a one-dimensional soil water model (VAMPS) and a three-component chemical mass-balance mixing model to describe the stormflow response of the catchment. It is inferred that most stormflow travelled through macropores in the top 20 cm of the soil profile. During a large event, saturation overland flow also accounted for a considerable portion of the stormflow, although it was not possible to quantify the associated volume fully. Although the mass-balance mixing model approach gave valuable information about the various flow paths within the catchment, it was not possible to distill the full picture from the model alone; additional hydrometric and soil physical evidence was needed to aid in the interpretation of the model results. Copyright © 2004 John Wiley & Sons, Ltd.

KEY WORDS runoff generation; rainforest; chemical mixing model; soil water model; geo-electrical survey

## INTRODUCTION

A fundamental concept in all studies of stormflow generation is the separation between fast and slow flow paths. The concept of how this is linked to hillslope processes has changed considerably since Horton (1933) first presented his infiltration-based model of runoff generation. The 'variable source concept' advanced by Hewlett and Hibbert (1967) also includes soil depth, slope position and morphology in the runoff generating process, as well as most superficial and subsurface flow types that have been observed in catchments throughout the world. However, later research (McDonnell, 1990; Brammer and McDonnell, 1996) has shown how the incorporation of new techniques, such as the use of stable isotopes, can change these conceptual views at the hillslope scale. Indeed, it is more or less accepted now that a combination of hydrometric and hydrochemical techniques is probably required to obtain a complete picture (Bonell and Fritsch, 1997). Macropores have been suggested to play a key role in the hydrological response of headwater catchments in general, and forested ones in particular (Beven and Germann, 1982; Bonell, 1993). Macropores are formed by the activities of soil fauna, root dynamics (growth, decay), the shrinking of clay, the erosive action of subsurface flow, or

* Correspondence to: J. Schellekens, Faculty of Earth and Life Sciences, Vrije Universiteit Amsterdam, De Boelelaan 1085, 1081 HV Amsterdam, The Netherlands. E-mail: schj@geo.vu.nl

*Received 8 January 2001*
*Accepted 13 February 2003*

combinations of the above (Jones, 1971; Beven and Germann, 1982; Lal, 1987). Macropores (especially 'pipes', i.e. macropores with a diameter exceeding 50 mm, Beven and Germann, 1982) may offer a fast flow path for water to the stream channel, depending on their size, frequency and the connectivity of the pores (Whipkey, 1965; Jones, 1971; Mosley, 1979; Mosley, 1982; Beven and Germann, 1982; Elsenbeer and Cassel, 1990).

The spatial variability in occurrence of macropores (including pipes), and thus hillslope hydraulic conductivity, is notorious (Jones, 1971; Elsenbeer and Lack, 1996; Brammer and McDonnell, 1996) and constitutes one of the main impediments to the successful application of physically based runoff generation models to predict stormflow characteristics (Smith and Hebbert, 1979; Loague and Kyriakidis, 1997; Merz and Plate, 1997; Vertessy and Elsenbeer, 1999). Despite the fact that the interest in, and imperatives for, the use of such models to forecast the hydrologic impacts of land-use change in the humid tropics has never been greater (Bruijnzeel, 1990, 1993; Jepma, 1995; Nepstad *et al.*, 1999), only a handful of in-depth studies of runoff generation have been conducted under such conditions (reviewed by Bonell (1993) and Bonell and Fritsch (1997)). Even fewer studies have attempted to model the runoff generation processes taking place on tropical hillsides, either before forest clearing (Molicova *et al.*, 1997; Chappell, 1998; Vertessy and Elsenbeer, 1999) or long after (Rose and Yu, 1998).

This paper offers a preliminary characterization of the hydrological response of one such tropical steepland catchment, the Bisley II catchment in the Luquillo Experimental Forest (LEF) in northeastern Puerto Rico, using a combination of hydrometric and hydrochemical (mass-balance mixing model) techniques. In addition, attention is paid to unravelling the subsurface structure of the catchment, notably the thickness of the saprolite and the depth to bedrock, as well as the identification of isolated micro-topographic depressions in the soil–bedrock interface that may store old water that may become remobilized when these depressions spill over during particularly wet spells (Brammer and McDonnell, 1996).

## STUDY CATCHMENT

The Bisley II catchment is situated at 18°18′N, 65°50′W at an elevation of 265–456 m a.s.l. (see Figure 1). The 6·4 ha catchment drains dissected mountainous terrain. Stream gradients in and around the catchment are steep, and hillslopes are generally convex–concave in form. The upper slope segments are convex, whereas middle sections are typically straight. The lower slope segments are usually concave when they pass into first-order valleys and straight where they join the main channel. More than half of the catchment has slopes greater than 45% (24°; Scatena, 1989). Shallow earth movement, soil creep and tree fall are important geomorphic processes in the area (Lewis, 1974, 1976; Simon *et al.*, 1990; Scatena and Larsen, 1991). The 0·8–1·0 m deep clayey soils that have developed in the underlying thick-bedded tuffaceous sandstones and indurated siltstones are strongly leached Ultisols. Silver *et al.* (1994) reported average soil bulk densities in the Bisley catchment area of 0·60 (0–10 cm), 0·98 (10–35 cm) and 1·30 g cm $^{-3}$ (35–60 cm). Similar values were obtained by Edmisten (1970) at nearby El Verde. Saturated hydraulic conductivity $K_{sat}$ in riparian zones in the Bisley area was estimated by McDowell *et al.* (1992) to range between 1 and 20 m day$^{-1}$ using an infiltrometer and between 0·009 and 0·09 m day$^{-1}$ using recovery tests in piezometer tubes. Additional soil physical data and the results of a geophysical survey to define subsurface bedrock topography will be presented later in the paper.

The Tabonuco-type rain forest of the study area has an irregularly shaped, 20–25 m high upper canopy, an understorey of palms and woody vegetation, and ground-level herbs and shrubs. Both the structure and composition of the vegetation vary with topography and aspect relative to the trade winds (Lugo and Scatena, 1995). The average leaf area index (LAI) of mature Tabonuco forest is between 6 and 7, but it has been reported to range between 12·1 on ridges and 1·95 in dark ravines and riparian valleys (Odum *et al.*, 1970). In September 1989 the Bisley area was severely impacted and nearly completely defoliated by Hurricane Hugo

 

(Scatena *et al.*, 1993). However, by 1996, when the present study was initiated, LAI and forest biomass were again similar to pre-hurricane conditions (Scatena *et al.*, 1996; Holwerda, 1997).

The climate is maritime tropical (type A2m according to the Köppen classification), with an annual rainfall of 3530 mm (as measured at the nearby long-term rainfall station at El Verde, 450 m a.s.l.). About 70% of the annual rainfall is associated with tropical waves, depressions and cyclones and is brought in with the northeasterly trade winds. Rainfall is distributed fairly evenly throughout the year, with May and November being relatively wet (>300 mm month$^{-1}$) and January–March relatively 'dry' (<200 mm month$^{-1}$). Rainfall at El Verde is delivered as numerous (267 rain days per year), relatively small (median daily rainfall 3·0 mm) storms of low intensity (<5 mm h$^{-1}$, Brown *et al.*, 1983; García-Martinó *et al.*, 1996). Schellekens *et al.* (1999) reported rainfall intensity for a 66 day study period between May and July 1996 to have a mean value of 3·0 mm h$^{-1}$ and a median value of 1·9 mm h$^{-1}$. Average rainfall interception is exceptionally high at *c*. 50%, regardless of storm size (Schellekens *et al.*, 1999).

The seasonal variation in mean monthly temperatures in the Bisley area is about 3·5 °C, ranging from 24 °C in December–February to about 27·5 °C in July–August. Seasonal variation in average daily relative humidity levels is small (84–90%). Average monthly wind speeds in the lower reaches of the LEF are <2 m$^{-1}$ s, but they vary between 2 and 5 m$^{-1}$ s around exposed summits at higher elevations (Brown *et al.*, 1983). Reference evaporation at Bisley has been estimated at *c*. 1100 mm year$^{-1}$ (Holwerda, 1997).

## METHODS

Stormflow generation at Bisley was investigated using various techniques. Previously, a detailed water budget evaluation of the catchment was performed (Schellekens *et al.*, 2000). In this study, it was supplemented by chemical analysis of different water types during periods of baseflow and stormflow. Furthermore, a geophysical survey was conducted to establish the subsurface characteristics of the catchment. The hydrometric data were used in combination with the soil and geophysical data and a one-dimensional soil water balance model VAMPS, Schellekens, 1997), to describe the stormflow response of the catchment quantitatively. Finally, the chemical tracer data were used in an application of a three-component mass-balance flow separation model (DeWalle *et al.*, 1988) to complete the picture. The remainder of this section describes the methods and associated instrumentation in more detail (see Figure 1 for locations).

A Texas Instruments tipping bucket rain gauge (TE525LL-L; 0·254 mm per tip) recorded above-canopy precipitation at 26 m. An adjacent totalizing rain gauge serving as a backup was emptied every week. The data were stored in a Campbell Scientific Ltd 21X data logger at 5 min intervals and retrieved weekly for further processing.

Throughfall (TF) was recorded continuously between 5 May and 9 July 1996 (66 days) using three flat-bottomed, sharp-rimmed steel gutters (6 cm × 300 cm) placed at a steep angle to minimize splash-out. Each gutter was equipped with a 180 l capacity tipping bucket and logger system. To minimize wetting and drying losses, the gutters were cleaned and sprayed with a silicone solution every week. In addition, TF was measured with 20 randomly placed but non-roving collectors (143 cm$^2$ surface area each), which were emptied every week. A roving gauge technique (Lloyd and Marques-Filho, 1988) had been adopted previously at Bisley, but after an initial comparison of the performance of fixed and roving gauges did not show significant differences only the fixed network was maintained (see Brouwer (1996)). The 5 min TF records obtained with the gutters were converted to areal averages every time the manual gauges were emptied, using a weighting procedure based on the relative magnitude of the surface areas of the respective gauge types. Stemflow was estimated as 2·3% of gross precipitation (Scatena, 1990b).

Stream water levels at the catchment outlet were measured at 5 min intervals using a Druck Ltd PDCR-830 pressure transducer (1·5 mm accuracy) connected to a CTL data logger. Water level measurements were made daily using a staff gauge to check for instrumental drift. Water level data were converted to discharge using a stage–discharge relation developed by Scatena (1990a). Four piezometers were installed in riparian areas that

 

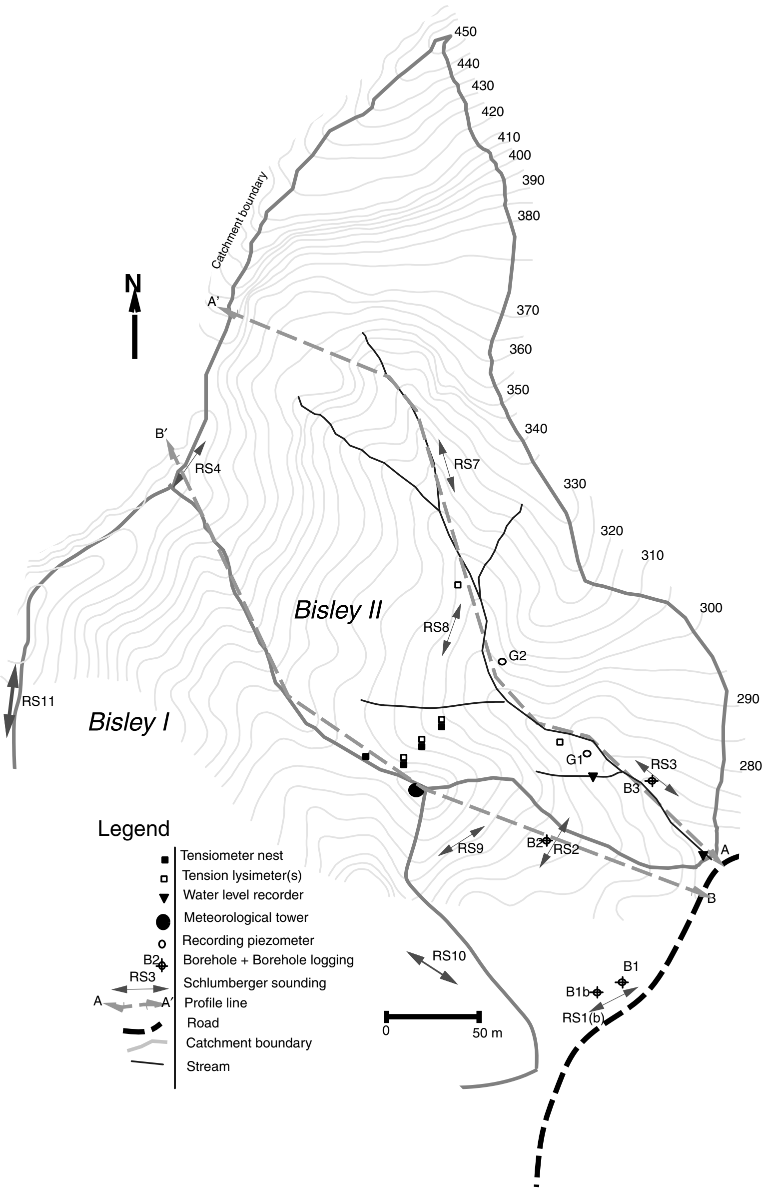


Figure 1. Map of the Bisley II catchment showing the location of Schlumberger soundings, instruments and profiles A–A′ and B–B′ as depicted in Figure 4

might contain groundwater and two of these were equipped with water-level recording equipment (pressure transducer connected to a data logger). A V-notch with a pressure transducer and logger was placed in a small tributary gully fed by return flow water during storms on 18 June 1996. Finally, volumes of quickflow and delayed flow at the catchment outlet were approximated using a simple straight-line separation method (Hewlett and Hibbert, 1967). A fixed slope of 0·025 mm $h^{-1}$ $day^{-1}$ was used in the separations.

Soil water retention characteristics, i.e. pairs of soil water content ($\theta$) and soil water tension ($\psi$) values, were obtained from undisturbed core samples (100 $cm^3$) using the porous-medium with pressure-membrane technique (Stakman, 1973). A total of 52 cores were used, distributed among three soil horizons (23 samples for the 0–20 cm interval, 18 between 20 and 50 cm and 11 between 50 and 140 cm). In addition, the cores were used to determine porosity, bulk density, and saturated hydraulic conductivity ($K_{sat}$) using a falling-head permeameter (Wit, 1962). Furthermore, a total of 13 reversed auger-hole method measurements of $K_{sat}$ (Van Beers, 1979) were also performed.

Soil water tension ($\psi$) was monitored using a nest of six tensiometers installed at a ridgetop (at 7, 19, 49, 67 and 84 cm depths) and three pairs of tensiometers (8 and 30 cm depths) along a single hillslope section. The instruments were read every 1–4 days using a needle plus transducer system accurate to the nearest centimetre. The maximum soil water tension that could be recorded was about 0·9 MPa (pF = 2·9). Values of $\psi$ were converted to soil water content $\theta$ using so-called Van Genuchten curves describing the $\psi$–$\theta$ pairs determined on the small cores (Mualem, 1976; Van Genuchten, 1980). Both soil water content and tension were simulated (using 5 min time steps) with the aid of the VAMPS model. Model predictions were calibrated against tensiometer readings made at several depths.

A total of ten Schlumberger geo-electrical soundings were performed throughout the catchment using a Terrameter (SAS 4000). The Gosh filter technique (Gosh, 1971; Koefoed, 1979) and non-linear regression (Marquardt, 1963) were used to derive an interpretation of subsurface structures according to a layered model (Telford *et al.*, 1976). In addition, three boreholes (6·75, 8·0 and 8·7 m deep) were made by hand using an auger. Laboratory determinations of the electric resistance and gravimetric water content of soil samples taken every 50 cm from these holes were done to validate the interpretation of the field soundings. For the same purpose, borehole logging using long- and short-normal electrodes (Telford *et al.*, 1976) was performed in two of the holes using the Terrameter. Amounts of acid-extractable calcium, magnesium, sodium, iron, manganese, potassium, and phosphorus were determined for soil samples from one of the boreholes at the International Institute of Tropical Forestry (IITF), Rio Piedras. After extraction by 1 M KCL (for calcium) or the modified Olsen method (for phosphorus and potassium), a Beckman plasma emission spectrometer was used for analysis of the extracts. A more detailed description of the analytical techniques can be found in Silver *et al.* (1994).

Samples for chemical analysis were also taken of the following water types: (1) precipitation (*P*), (2) floodplain groundwater (GW), (3) streamflow (both during storms (STF) and during baseflow conditions (BF)), (4) return flow/gully flow (RF) and (5) soil water (SW). For each sample, two polyethylene bottles were used. Each bottle had been rinsed with a 10% $HNO_3$ solution to remove any adsorbed ions before rinsing six times with distilled water. The first bottle (50 ml) was acidified. Before acidifying (with 0·7 ml of 65% $HNO_3$) the sample was filtered using a 50 μm micropore filter. The second bottle (250 ml) was never filtered or acidified. The streamflow sample bottles were rinsed another six times using streamwater prior to sampling. For samples that were large enough (e.g. all stream water samples) a third non-acidified sample was taken. These sample were analysed in the field laboratory with a week using a portable titration kit for chloride, calcium, magnesium and $HCO_3^-$. In addition, electrical conductivity (EC) and pH were also determined at that time. All samples were stored at 4 °C. The longest time between sampling and analysis for any sample was 1 month. All samples were transported to the Vrije Universiteit Amsterdam in checked-in luggage and arrived at the laboratory within 12 h. In total, 102 samples were analysed at the Vrije Universiteit Amsterdam for calcium, magnesium, silicon, potassium, sodium and chloride using a Perkin Elmer (model 6500) inductively coupled plasma photometric (calcium, magnesium, silicon), flame photometric (potassium, sodium) and auto-analyser (chloride) techniques. EC was determined in the field as well as in the laboratory.

Selected pairs of the constituents analysed were used in a three-component flow separation model (DeWalle *et al.*, 1988). Although temporal and spatial variations in the concentrations of chemical constituents in incident precipitation during a storm event exist (Kendall and McDonnell, 1993), these were neglected in the present research. For a three-component mixing model, the relative contribution (fraction) of each source to total streamflow can be obtained by solving the following set of equations (DeWalle *et al.*, 1988; Genereux *et al.*, 1993):

$$
\begin{aligned}
f_1 + f_2 + f_3 &= 1 \\
[A]_1 f_1 + [A]_2 f_2 + [A]_3 f_3 &= [A]_s \\
[B]_1 f_1 + [B]_2 f_2 + [B]_3 f_3 &= [B]_s \qquad (1)
\end{aligned}
$$

where $f$ is the fraction contributed by each flow component, [A] is the concentration (μeq $l^{-1}$) of constituent A and [B] the concentration (μeq $l^{-1}$) of constituent B.

The subscript 's' denotes streamflow, and the subscripts 1, 2 and 3 refer to the different flow components (sources).

## RESULTS

### *Geophysics*

Although the combination of steep slopes and dense vegetation rendered the laying out of Schlumberger arrays difficult, the resulting resistivity curves allowed unambiguous interpretation (Figure 2). In some cases, lateral changes in the subsurface structure caused some shift in the upper part of the curves (for values of *L*/2 < 4 m), but this did not affect the interpretation. As illustrated in Figure 2, in which four soundings within the main valley are shown, a layer of high resistivity occurs below depths of 23–30 m. This is overlain by a

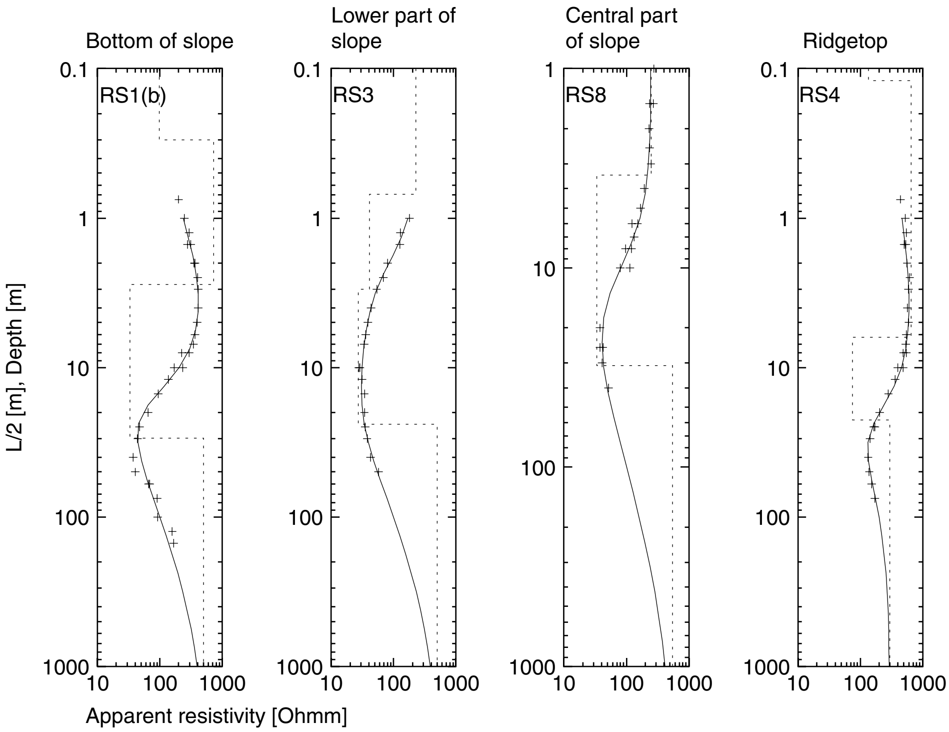


Figure 2. Schlumberger soundings of the substrate along four transects in the Bisley II catchment (see Figures 1 and 4 for locations and topographic setting). Plus signs (+) represent measured resistivity values (Ω m), the solid line the fitted curve, and the dotted line the resulting layered model representation of the substrate. The vertical axis shows *L*/2 (the length of the Schlumberger array) and the depth of the layered model, both are in metres

 

layer of much lower resistivity, starting typically at a depth of 3–3·5 m for the lower to central portion of the river profile, to *c*. 6 m below the highest point. On top of this intermediate zone of low resistivity lies a layer of variable thickness and intermediate to high resistivity values (Figure 2). Figure 3 compares the resistivity profiles with depth for one of the boreholes, RS1b, located near the outlet of the catchment (see Figures 1 and 4 for location and setting). The changes in soil nutrient concentrations in the top 50 cm and below 5–6 m (Figure 3B) show the opposite pattern derived for resistivity (Figure 3A). Conversely, no clear relationships are observed between gravimetric soil water content (Figure 3C) and either soil chemistry (Figure 3B) or resistivity (Figure 3A). Similar findings were obtained for the other two boreholes (Van Dijk *et al.*, 1997). On the basis of the ten Schlumberger soundings distributed over the catchment and the measurements made in the three boreholes, a generalized subsurface profile was constructed for the Bisley II catchment (Figure 4). The deepest zone of high resistivity is thought to represent the non-weathered bedrock, which is generally found at depths exceeding 20 m. The intermediate zone of low resistivity values represents the saprolite (rotten rock), which grades into highly leached saprolite/sub-soil material of higher resistivity values and low nutrient contents, typically at a depth of 3–6 m (see Figure 3B). Interestingly, the transitions between fresh and weathered bedrock, and between the latter and subsoil material, closely follow the longitudinal profile of the streambed rather than run parallel to the surface topography (Figure 4).

*Soil physical parameters*

Soil hydraulic conductivity ($K_{sat}$) ranged from 0·01 to 7·33 m day$^{-1}$, depending on depth and the method used (Table I). The range is especially large for the 0–20 and 20–50 cm horizons, causing median values to be 25–70 times lower than arithmetic average values. This large scatter in $K_{sat}$ values undoubtedly reflects the relative frequencies of macropores in the small core samples, as also evidenced by the much higher $K_{sat}$ values obtained with the reverse auger hole method, despite the fact that the latter method tends to underestimate

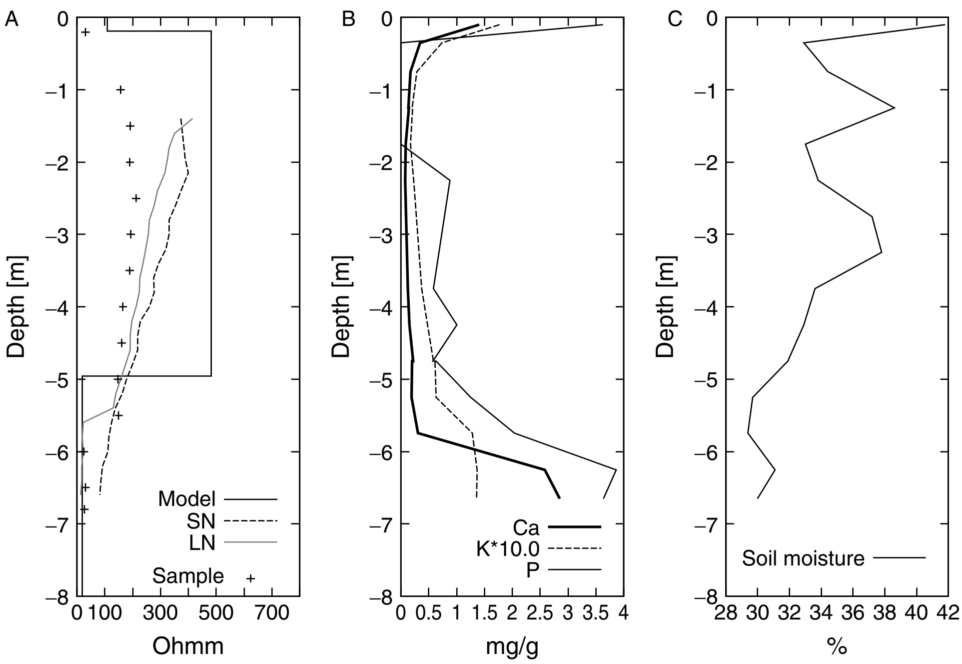


Figure 3. Variations with depth for various parameters as determined in borehole RS1b (bottom of slope; see Figure 1 for location). (A) Interpreted layered model from the Schlumberger sounding (solid line) plus the results from the borehole logging (long- and short-normal, LN, SN) and measured sample resistivities (+). (B) Concentrations of calcium, potassium and phosphorus in soil samples taken at 50 cm intervals. (C) Gravimetric moisture content (%)

 

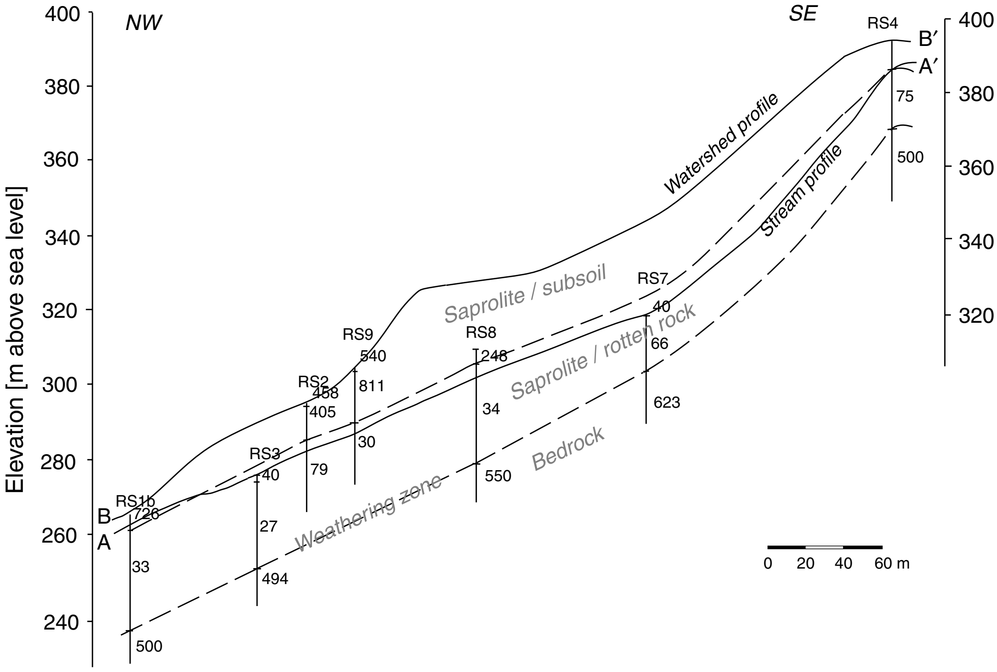


Figure 4. NW–SE profile of the subsurface of the Bisley II catchment showing the locations of the Schlumberger resistivity soundings (indicated by vertical bars with their location code; the numbers along the bars are resistivities (Ω m) and the interpreted layered structure as indicated by the dashed lines. Also indicated (by solid lines) are the catchment topographical profile, as measured along the ridge, (B–B′) and the streambed profile (A–A′). The locations of both profile lines are indicated in Figure 1

$K_{sat}$ in clayey soils due to smearing of the holes (Kessler and Oosterbaan, 1973). The associated confidence limits reflect the highly variable nature of the $K_{sat}$ data. The $K_{sat}$ estimates for the auger hole show a clear decrease with depth, and the confidence limits for the median between 0–20 and 20–50 cm do not overlap. For the small core sample the picture is less clear, and confidence limits overlap for the entire depth range. However, assuming that the auger hole method gives a better estimate (given the larger sample size), a decline of $K_{sat}$ in depth can be assumed for the Bisley catchment. This apparent decrease in $K_{sat}$ with depth (auger hole values for the top 50 cm, small core samples for the subsoil) is paralleled by a decrease in porosity and an increase in bulk density below 50 cm (Table I). Nevertheless, at 50% the porosity of the soil below 50 cm depth is still quite high.

*Soil water tension*

Using previously established 5 min rainfall interception and transpiration totals (Schellekens *et al*., 1999, 2000), the one-dimensional VAMPS site water balance model (Schellekens, 1997) was run to simulate soil water tensions at different depths at a near-level ridgetop site between 5 May and 15 July 1996. Time steps of 5 min were used. The Van Genuchten curves used in the model runs were the same for each of the three soil layers. Macropore flow was not explicitly taken into account by the model. Instead, an approximate approach was used in which lateral drainage (both saturated and unsaturated) out of the modelled soil column was permitted at rates governed by the prevailing hydraulic conductivity (saturated or unsaturated, depending on the moisture conditions in each node) and the average slope angle of the site. Measured tension values at 7, 18, 36, 49, 67 and 84 cm depths were available from 17 June until 11 July, against which model predictions were tested after averaging the results within each of the three soil layers (Figure 5). During the virtually rainless period between 22 June and 6 July, soil water tensions at 7 cm depth increased to 813 cm versus 281 cm at 49 cm

 

Table I. Saturated hydraulic conductivity ($K_{sat}$) as determined on small core samples and according to the reversed auger-hole method for three soil layers in the Bisley II catchment. Porosity and bulk density were determined on small core samples only

| Depth (cm) | $K_{sat}$ m day$^{-1}$ | | | Confidence limits (0·9) | | $n$ | Bulk density (g cm$^{-3}$) | | | Confidence limits (0·9) | | $n$ | Porosity | | | Confidence limits (0·9) | | $n$ |
|---|---|---|---|---|---|---|---|---|---|---|---|---|---|---|---|---|---|---|
| | Min. | Max. | Median | Upper | Lower | | Min. | Max. | Median | Upper | Lower | | Min. | Max. | Median | Upper | Lower | |
| *Small cores* | | | | | | | | | | | | | | | | | | |
| 0–20 | $2·38 \times 10^{-4}$ | 3·59 | $1·73 \times 10^{-3}$ | 0·44 | −0·43 | 21 | 0·62 | 1·32 | 0·87 | 0·99 | 0·76 | 10 | 0·53 | 0·74 | 0·66 | 0·70 | 0·63 | 10 |
| 20–50 | $8·42 \times 10^{-4}$ | 6·83 | $1·25 \times 10^{-2}$ | 0·68 | −0·66 | 19 | 0·81 | 1·13 | 0·90 | 0·98 | 0·81 | 7 | 0·56 | 0·68 | 0·64 | 0·67 | 0·62 | 7 |
| 50–140 | $1·71 \times 10^{-4}$ | 0·11 | $3·94 \times 10^{-3}$ | 0·02 | −0·01 | 11 | 0·98 | 1·32 | 1·18 | 1·27 | 0·89 | 7 | 0·53 | 0·65 | 0·57 | 0·60 | 0·54 | 7 |
| *Auger hole* | | | | | | | | | | | | | | | | | | |
| 0–20 | 0·13 | 11·79 | 7·33 | 11·82 | 2·84 | 5 | | | | | | | | | | | | |
| 20–50 | 0·10 | 1·52 | 0·69 | 1·04 | 0·33 | 8 | | | | | | | | | | | | |
| *Small cores + Auger hole* | | | | | | | | | | | | | | | | | | |
| 0–20 | $2·38 \times 10^{-4}$ | 11·79 | 0·02 | 1·07 | −1·03 | 26 | | | | | | | | | | | | |
| 20–50 | $8·42 \times 10^{-4}$ | 6·83 | 0·13 | 0·60 | −0·34 | 27 | | | | | | | | | | | | |
| 50–140 | $1·71 \times 10^{-4}$ | 0·11 | $3·94 \times 10^{-3}$ | 0·02 | −0·01 | 11 | | | | | | | | | | | | |

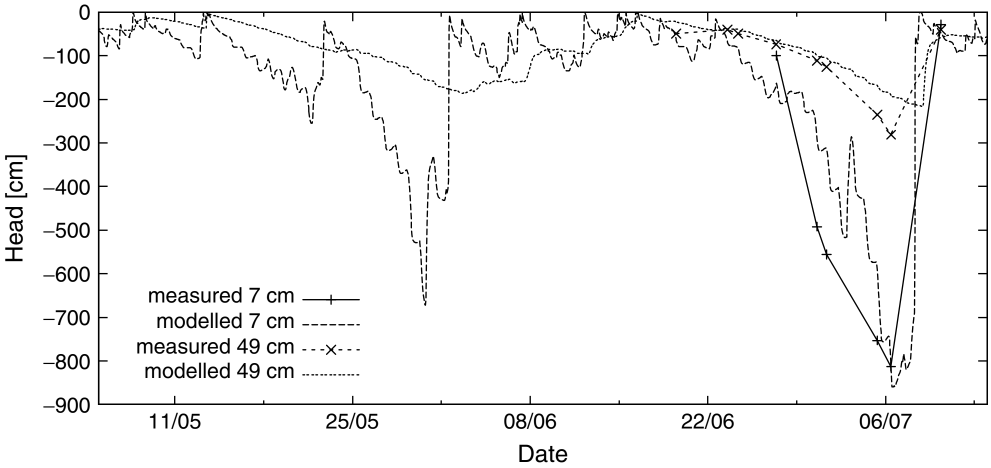


Figure 5. Measured and modelled soil water tension at two depths on a ridge top location between 5 May and 15 July 1996. The last part of the graph includes measured data that were used to calibrate the model

depth and only 145 cm at 83 cm depth. The decline in $K_{sat}$ (and rooting density, see Edmisten (1970)) with depth, notably below 50 cm, caused soil water tension to remain relatively high throughout the simulation period (Figure 5). Best fits between measured and modelled soil water tensions at the three depths (two of which are shown in Figure 5) were obtained for optimized $K_{sat}$ values of 3·6, 1·2 and 0·06 m day$^{-1}$ for the respective layers. These values were within the range of actual fields measurements (Table I).

*Straight-line flow separation*

Average quickflow amounts were determined using the simple straight-line separation method for 31 storms occurring in the period 19 April–9 July 1996 (Table II). Maximum quickflow depth (63·8 mm) occurred in response to an exceptionally large (228 mm of gross precipitation) storm (no. 16) starting on 13 May for which quickflow lasted for 24 h 38 min. The corresponding quickflow/rainfall ratio was 0·28. The lowest quickflow volume (0·01 mm) was observed for a 7·8 mm storm (no. 45) falling on 25 May, which produced a quickflow/rainfall ratio of only 0·02 (Table II). The characteristics associated with the 31 storms listed in Table II are examined further in Table III in terms of their dependence on rainfall amount and intensity, as well as antecedent soil water status as simulated using the VAMPS model (see Figure 5). Both quickflow volume (column 4 in Table III) and peak discharge (column 2) turn out to be closely related to storm rainfall total (variable no. 7) but much less to average rainfall intensity (variable no. 8). A rather striking finding is the absence of strong (or even modest) correlations between key storm hydrograph parameters and a range of parameters describing antecedent wetness conditions, such as soil moisture content or the precipitation for various periods preceding the storm (variables nos. 9–19).

*Piezometer and gully response*

Stormflows emerging as return flow in a small tributary gully (see Figure 1 for location) were seen to react faster to instantaneous changes in throughfall intensity than the water levels at the catchment outlet (Figure 6A). Generally, the delay between the peak in throughfall intensity and maximum discharge in the gully was less than 5 min (Figure 6A). A comparison of the flow record for the gully with simulated soil water tensions in the top 10 cm of the soil (Figure 7A and B) shows that the soil is very wet (tensions <50 cm) when the gully starts to carry water, although it does not reach full saturation. Interestingly, the timing of the flow in the gully coincides closely with the occurrence of lateral drainage from the top 10 cm of the soil as inferred from the VAMPS model simulations (Figure 7B).

 

Table II. Basic characteristics of 31 storms selected from the Bisley II streamflow record between 19 April and 9 July 1996. Italic and bold values indicate maximum and minimum values respectively

| Date | Storm no. | *P* (mm) | Quickflow duration (days) | Peak flow (mm/5 m) | Total flow (mm) | Quickflow (mm) | Delayed flow (mm) | QF/*P* |
|---|---|---|---|---|---|---|---|---|
| 23/04 | 2 | — | 0·61 | 0·48 | 27·67 | 8·11 | 19·56 | — |
| 26/04 | 5 | — | 0·29 | 0·02 | 2·38 | 0·58 | 1·80 | — |
| 30/04 | 9 | — | 0·28 | 0·09 | 2·59 | 1·11 | 1·48 | — |
| 06/05 | 11 | 8·84 | 0·21 | 0·02 | 1·37 | 0·34 | 1·03 | 0·04 |
| 07/05 | 12 | 31·24 | 0·38 | 0·38 | 18·95 | 4·82 | 14·14 | 0·15 |
| 08/05 | 13 | 14·81 | 0·29 | 0·17 | 4·57 | 2·52 | 2·05 | 0·17 |
| 09/05 | 14 | 5·76 | 0·21 | 0·02 | 1·95 | 0·35 | 1·60 | 0·06 |
| 13/05 | 16 | *227·53* | *1·37* | *2·93* | *96·43* | *63·81* | *32·62* | *0·28* |
| 21/05 | 19 | 5·71 | 0·13 | 0·02 | 1·80 | 0·09 | 1·70 | 0·02 |
| 22/05 | 20 | **3·23** | **0·10** | 0·02 | 1·53 | 0·08 | 1·45 | 0·03 |
| 22/05 | 21 | 16·34 | 0·23 | 0·10 | 5·01 | 1·39 | 3·62 | 0·09 |
| 23/05 | 22 | 4·07 | 0·15 | 0·03 | 1·15 | 0·32 | 0·82 | 0·08 |
| 24/05 | 23 | 3·36 | 0·10 | **0·01** | **0·95** | **0·07** | 0·87 | 0·02 |
| 01/06 | 25 | 24·41 | 0·26 | 0·19 | 5·21 | 2·38 | 2·83 | 0·10 |
| 02/06 | 26 | 15·95 | 0·27 | 0·09 | 3·06 | 1·34 | 1·72 | 0·08 |
| 06/06 | 28 | 9·74 | 0·20 | 0·03 | 2·75 | 0·59 | 2·15 | 0·06 |
| 07/06 | 29 | 38·54 | 0·53 | 0·18 | 13·56 | 4·59 | 8·97 | 0·12 |
| 08/06 | 30 | 4·36 | 0·16 | 0·03 | 1·02 | 0·31 | **0·72** | 0·07 |
| 11/06 | 32 | 40·14 | 0·61 | 0·28 | 13·34 | 4·55 | 8·79 | 0·11 |
| 14/06 | 37 | 20·46 | 0·30 | 0·13 | 5·86 | 2·38 | 3·48 | 0·12 |
| 15/06 | 38 | 10·83 | 0·22 | 0·07 | 2·63 | 1·21 | 1·42 | 0·11 |
| 15/06 | 39 | 12·74 | 0·24 | 0·15 | 3·49 | 1·84 | 1·65 | 0·14 |
| 16/06 | 40 | 54·76 | 0·58 | 0·49 | 24·60 | 12·56 | 12·04 | 0·23 |
| 18/06 | 41 | 8·00 | 0·13 | 0·05 | 1·26 | 0·48 | 0·78 | 0·06 |
| 18/06 | 42 | 11·82 | 0·24 | 0·08 | 2·73 | 1·00 | 1·72 | 0·08 |
| 18/06 | 43 | 5·06 | 0·13 | 0·03 | 1·38 | 0·25 | 1·13 | 0·05 |
| 21/06 | 44 | 5·82 | 0·15 | 0·03 | 2·03 | 0·28 | 1·75 | 0·05 |
| 22/06 | 45 | 7·83 | 0·16 | 0·02 | 3·96 | 0·10 | 3·86 | **0·01** |
| 22/06 | 46 | 12·77 | 0·24 | 0·12 | 3·21 | 1·20 | 2·01 | 0·09 |
| 08/07 | 49 | 17·80 | 0·20 | 0·08 | 3·22 | 1·20 | 2·02 | 0·07 |
| 08/07 | 50 | 61·41 | 0·50 | 0·48 | 15·83 | 12·65 | 3·18 | 0·21 |
| Mean | 28·10 | 22·04 | 0·30 | 0·22 | 8·89 | 4·27 | 4·61 | 0·09 |
| Median | 28·00 | 10·83 | 0·24 | 0·08 | 3·06 | 1·20 | 1·80 | 0·09 |
| Stdev | 13·90 | 41·10 | 0·25 | 0·52 | 17·71 | 11·53 | 6·82 | 0·06 |

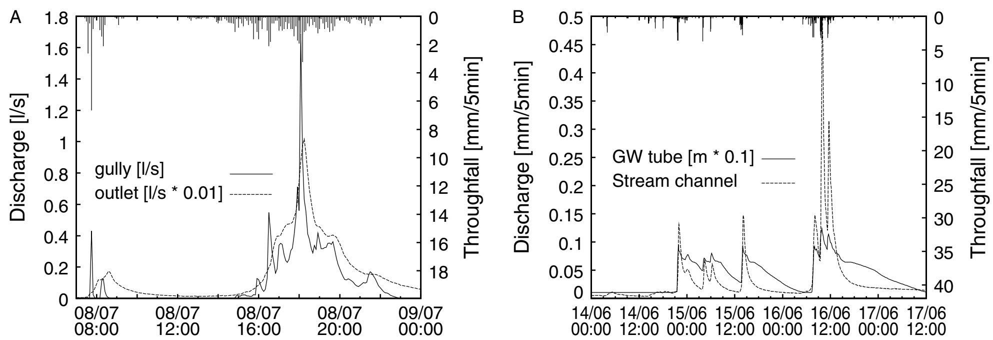


Figure 6. (A) Discharge in the creek and in a small tributary gully for two rainfall events in July 1996 (note: creek discharge is divided by 100 for scaling purposes). (B) Reaction of groundwater levels in piezometer G1 compared with the water level in the creek

 

Table III. Correlation (*r* linear) matrix of storm parameters. For clarity, all coefficients smaller than 0·15 have been replaced by a dash. Columns headers, **1**: quickflow duration; **2**: peak flow; **3**: total flow; **4**: quickflow amount; **5**: baseflow amount; **6**: quickflow/total flow ratio; **7**: total precipitation; **8**: average precipitation intensity; **9**: precipitation during the previous day; **10**: precipitation in the previous week; **11**: initial soil moisture (0–20 cm); **12**: initial soil moisture (20–50 cm); **13**: initial soil moisture (50–140 cm); **14**: soil moisture on the previous day (0–20 cm); **15**: Soil moisture on the previous day (20–50 cm); **16**: soil moisture on the previous day (50–140 cm); **17**: average soil moisture in the previous week (0–20 cm); **18**: average soil moisture in the previous week (20–50 cm); **19**: average soil moisture previous in the week (50–140 cm); **20**: initial discharge; **21**: discharge at end of storm

| | **1** | **2** | **3** | **4** | **5** | **6** | **7** | **8** | **9** | **10** | **11** | **12** | **13** | **14** | **15** | **16** | **17** | **18** | **19** | **20** | **21** |
|---|---|---|---|---|---|---|---|---|---|---|---|---|---|---|---|---|---|---|---|---|---|
| **1** | 1·00 | | | | | | | | | | | | | | | | | | | | |
| **2** | 0·68 | 1·00 | | | | | | | | | | | | | | | | | | | |
| **3** | 0·75 | 0·99 | 1·00 | | | | | | | | | | | | | | | | | | |
| **4** | 0·69 | 1·00 | 0·99 | 1·00 | | | | | | | | | | | | | | | | | |
| **5** | 0·80 | 0·92 | 0·96 | 0·91 | 1·00 | | | | | | | | | | | | | | | | |
| **6** | 0·47 | 0·49 | 0·46 | 0·50 | 0·36 | 1·00 | | | | | | | | | | | | | | | |
| **7** | 0·76 | 0·99 | 0·99 | 0·99 | 0·93 | 0·54 | 1·00 | | | | | | | | | | | | | | |
| **8** | 0·32 | 0·70 | 0·69 | 0·71 | 0·61 | 0·63 | 0·73 | 1·00 | | | | | | | | | | | | | |
| **9** | — | — | — | — | −0·16 | 0·41 | — | — | 1·00 | | | | | | | | | | | | |
| **10** | −0·17 | — | — | — | — | — | — | — | — | 1·00 | | | | | | | | | | | |
| **11** | — | — | — | — | — | — | — | −0·16 | 0·48 | 0·61 | 1·00 | | | | | | | | | | |
| **12** | — | — | — | — | — | — | — | — | 0·24 | 0·67 | 0·85 | 1·00 | | | | | | | | | |
| **13** | — | — | — | — | — | −0·33 | — | −0·17 | — | 0·28 | 0·45 | 0·71 | 1·00 | | | | | | | | |
| **14** | — | — | — | — | — | — | — | −0·26 | 0·41 | 0·58 | 0·94 | 0·88 | 0·51 | 1·00 | | | | | | | |
| **15** | — | — | — | — | — | — | — | — | — | 0·69 | 0·79 | 0·99 | 0·76 | 0·83 | 1·00 | | | | | | |
| **16** | — | — | — | — | — | −0·37 | — | −0·15 | −0·18 | 0·26 | 0·38 | 0·64 | 0·99 | 0·43 | 0·70 | 1·00 | | | | | |
| **17** | — | — | — | — | — | −0·22 | — | — | — | 0·66 | 0·78 | 0·94 | 0·77 | 0·82 | 0·95 | 0·73 | 1·00 | | | | |
| **18** | — | — | — | — | — | −0·28 | — | — | — | 0·46 | 0·55 | 0·82 | 0·91 | 0·58 | 0·86 | 0·89 | 0·89 | 1·00 | | | |
| **19** | — | — | — | — | — | −0·47 | — | −0·28 | −0·19 | −0·23 | 0·08 | 0·25 | 0·81 | — | 0·30 | 0·83 | 0·38 | 0·65 | 1·00 | | |
| **20** | −0·51 | −0·22 | −0·25 | −0·21 | −0·32 | — | −0·28 | — | — | 0·66 | 0·49 | 0·57 | 0·38 | 0·40 | 0·56 | 0·38 | 0·49 | 0·50 | — | 1·00 | |
| **21** | — | 0·56 | 0·54 | 0·57 | 0·46 | 0·26 | 0·51 | 0·61 | — | 0·56 | 0·38 | 0·53 | 0·41 | 0·32 | 0·56 | 0·41 | 0·49 | 0·49 | — | 0·64 | 1·00 |

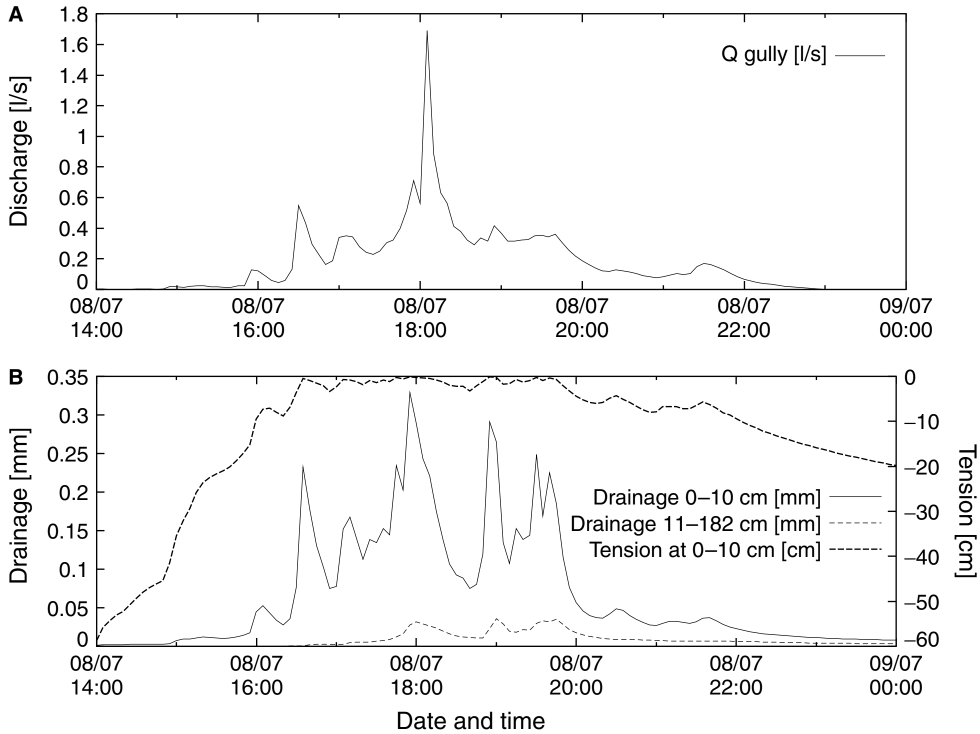


Figure 7. (A) Discharge from a tributary gully; (B) simulated soil water tensions in the top 10 cm and lateral drainage from the 0–10 and 11–182 cm horizons

The level of shallow groundwater as determined in piezometer G1 is seen to rise at the same time as the level of the creek, and at times even earlier (Figure 6B). The location of the piezometer tube with respect to the stream (Figure 1) and the magnitude of the fluctuations (the rise in the creek is about an order of magnitude smaller) rule out any direct influence by the water level in the creek. As will be discussed in more detail later, these rapid fluctuations in shallow groundwater levels relate to contributions by lateral macropore flow.

*Chemical composition of the different water types*

In support of the hydrometric observations, a total of 102 samples were taken of the various water types within the catchment. In particular, two storms were sampled in detail, including an extreme event occurring on 13 May (storm no. 16) and a smaller event occurring on 7 June (part of storm no. 29 in Table II). The corresponding quickflow (QF) amounts were 63·8 and 4·6 mm and the quickflow ratios (QF/P) 0·28 and 0·12 respectively. In general, the concentrations of the various constituents in the samples were low, with the lowest concentrations found in precipitation and the highest in streamflow during periods of baseflow (Table IV).

Based on the average EC, the respective contributing water types ranked in the following sequence for their overall solute concentrations: baseflow (BF) > shallow groundwater (GW) > matrix soil water (SW) > return flow (RF) > rainfall (P), although different rankings were sometimes obtained for certain elements (e.g. potassium, for which flow types such as return flow and shallow groundwater had relatively high concentrations (Table IV)). The concentrations of silicon (Si) showed the widest range in the different water types, with very little silicon in precipitation and by far the highest values during baseflow conditions. Intermediate values were found in SW and GW, whereas relatively low concentrations were also determined for return flow (gully

 

Table IV. Mean concentrations (meg/l: Ca, Mg, K, Na, Cl; meg/l: Si4*) of chemical constituents, pH and (μS $cm^{-1}$) sorted by water type. P: precipitation; SW: matrix soil water; RF: return flow (small gully); GW: shallow groundwater from piezometer; BF: streamwater (baseflow); STF: streamwater (during storms)

| Type | No. samples | | pH | EC | Si | Ca | Mg | K | Na | Cl |
|---|---|---|---|---|---|---|---|---|---|---|
| P | 3 | Mean | 5·5 | 20 | 15 | 75 | 12 | 14 | 85 | 92 |
| SW | 37 | Mean | 5·3 | 55 | 493 | 40 | 45 | 20 | 257 | 301 |
| | | Min. | 3·8 | 40 | 271 | 8 | 24 | 5 | 133 | 133 |
| | | Max. | 6·9 | 81 | 1207 | 150 | 110 | 111 | 382 | 500 |
| RF | 8 | Mean | 5·8 | 41 | 178 | 105 | 40 | 53 | 172 | 214 |
| | | Min. | 5·7 | 29 | 130 | 48 | 23 | 42 | 115 | 171 |
| | | Max. | 5·9 | 46 | 222 | 156 | 59 | 63 | 251 | 241 |
| GW | 7 | Mean | 5·5 | 58 | 487 | 167 | 67 | 61 | 191 | 240 |
| | | Min. | 5·1 | 48 | 279 | 69 | 50 | 16 | 131 | 160 |
| | | Max. | 6 | 68 | 691 | 290 | 86 | 119 | 243 | 321 |
| BF | 9 | Mean | 7 | 94 | 1913 | 303 | 125 | 34 | 301 | 216 |
| | | Min. | 6·5 | 75 | 1671 | 221 | 92 | 29 | 270 | 209 |
| | | Max. | 7·3 | 102 | 2209 | 351 | 146 | 41 | 339 | 224 |
| STF | 36 | Mean | 6·9 | 57 | 838 | 178 | 68 | 34 | 201 | 180 |
| | | Min. | 5·6 | 30 | 249 | 76 | 31 | 23 | 131 | 125 |
| | | Max. | 7·4 | 93 | 2035 | 316 | 134 | 45 | 328 | 233 |

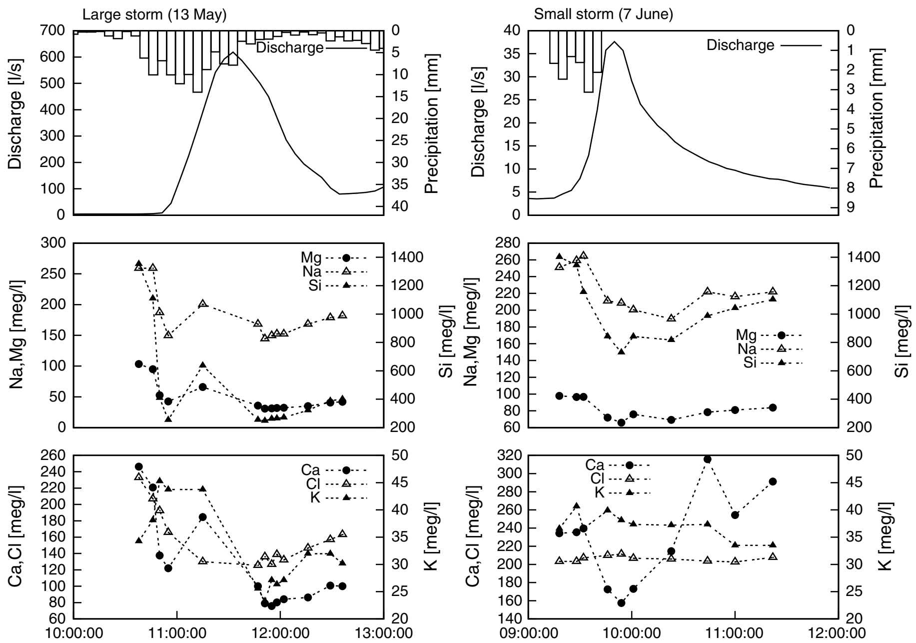


Figure 8. Dilution/enrichment patterns for streamwater concentrations of calcium, magnesium, silicon, potassium, sodium and chloride during two storm events at Bisley. The large event occurred on 13 May 1996, the smaller event on 7 June 1996

water). Consequently, the clear dilution patterns observed for silicon during the two storm events must reflect contributions by water types with low concentrations, especially during the largest event (Figure 8).

The lowest calcium concentrations were found in precipitation and soil water, and to a lesser extent in return flow (Table IV). During both storm events the calcium concentrations diminished rapidly during the first part of the storm, indicating an increase in contributions by one or more sources low in calcium (soil water, precipitation or return flow), although concentrations exceeded pre-storm levels at the end of the smaller event (Figure 8). A similar behaviour was shown by concentrations of magnesium and sodium, although soil water was more enriched in this case compared with precipitation. Again, concentrations of magnesium and sodium decreased during both storm events, indicating increased contributions by rain and return flow.

Potassium concentrations showed a markedly different pattern, with the highest concentrations occurring in return flow and shallow groundwater, indicating a near-surface source of potassium enrichment, such as litter leaching (Burghouts *et al*., 1998). The behaviour of potassium during the two storm events differed accordingly: concentrations in the stream initially increased (indicating a larger contribution of either return flow or shallow groundwater) before dropping below pre-storm levels (Figure 8).

Chloride (Cl) concentrations were highest in soil water and lowest in precipitation. During the smaller storm event Cl concentrations rose slightly during the initial phase and then dropped to about half the pre-storm concentration during the remainder of the event. As Cl is not present in appreciable quantities in the soil material itself, the increase is due to dry deposition and concentration due to evapotranspiration. Assuming a 50% increase in concentration due to interception losses and a 15% increase due to transpiration (Schellekens *et al*., 2000), one would expect the Cl concentration in BF to be about 271 meg $l^{-1}$ $(95/(1 - 0{\cdot}5 - 0{\cdot}15))$ and in STF to be about 190 meg $l^{-1}$ $(95/(1 - 0{\cdot}5))$. However, these simple assumptions disregard any temporal variations in the Cl content of the precipitation between and during storms, which may be high (*CF* Turvey, 1974).

*Mass-balance-based flow separation*

Mixing-plots of hydrochemical constituent pairs in streamflow, such as Figure 9, can be used to identify those constituent pairs that provide the best contrast between potentially contributing water types for subsequent use in a mass-balance flow separation model (Elsenbeer *et al*., 1995a). The following points emerge from Figure 9. (1) Stream water during baseflow is needed as the end member providing the highest concentrations of calcium, silicon, magnesium and sodium. (2) other useful end members include soil water, precipitation, return (gully) flow and shallow groundwater as sampled from the piezometers. The latter two water types, however, show very similar concentrations (except for silicon, Table IV) and are mostly of the same origin (*CF* Figure 6B). (3) Having the lowest concentrations, precipitation is also needed as an end member to represent an additional fast flow component next to return (gully) flow.

To apply a mass-balance flow separation model successfully the water types used as end members must differ significantly for the chosen constituent. The three-component mass-balance flow separation model (Equation (1)) was run for the two storms using all the constituent pairs displayed in Figure 9, *viz*. Cl–K, Na–K, Mg–K, Si–K, Ca–K, Si–Cl, Cl–Mg and Cl–Ca, albeit not always with the same end members. For Cl–K, Na–K, Si–Cl, Cl–Mg, Mg–K and Cl–Ca the end members used were P, RF and BF. For the remaining constituent pairs, SW, RF and BF were used as end members.

The results for the two storms are presented in Figures 10 and 11 and summarized in Table V. The different magnitude of the two events (228 versus 14·3 mm of rain) is clearly borne out in Figures 10 and 11. As expected, fast components like RF and P accounted for a much greater part of the total flow in the large event. Also, based on the Si–K and K–Ca pairs, the soil water contribution for the large event was estimated at more than 50% of the total flow (with a maximum of about 100% about midway on the falling limb of the hydrograph) versus only about 20% for the smaller event (Table V and Figure 10). Similar values were obtained for the estimated baseflow contribution based on the same constituent pairs. For the other constituent pairs, matrix soil water could not be used as an end member and precipitation P was used instead. As expected, the influence of P proved rather small for the smaller event (about 10%) whereas an average of about 40% was calculated for the large event. Calculated contributions by the RF component (gully water) varied between 27 and 41% for the smaller event and 24 to 54% for the large event, depending on constituent pair (Figures 10 and 11).

 

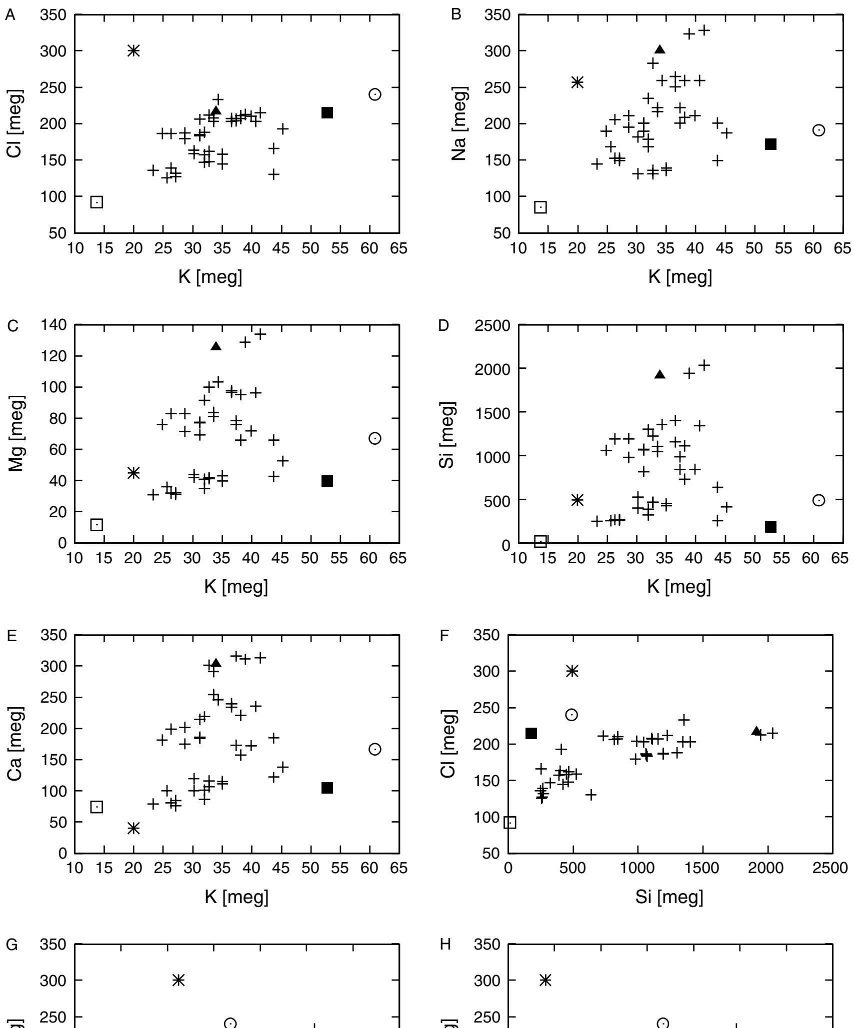


Figure 9. Selected mixing diagrams for hydrochemical constituent pairs in stream water at Bisley. Potential end members indicated by: ✳ = mean soil moisture, ■ = mean return flow (gully), ⊡ = mean precipitation ⊙ = mean shallow groundwater, ▲ = mean of stream water at baseflow conditions, + = stream water during stormflow conditions

## DISCUSSION

### *Catchment subsurface structure and soil physical properties*

The consistency between the results obtained with the Schlumberger measurements of resistivity with depth throughout the catchment (Figure 2), the borehole logs, and the sample resistivity analysis (Figure 3) suggests a four-layer subsurface structure for the Bisley II catchment: (i) a thin top layer of soil with low resistivity (10

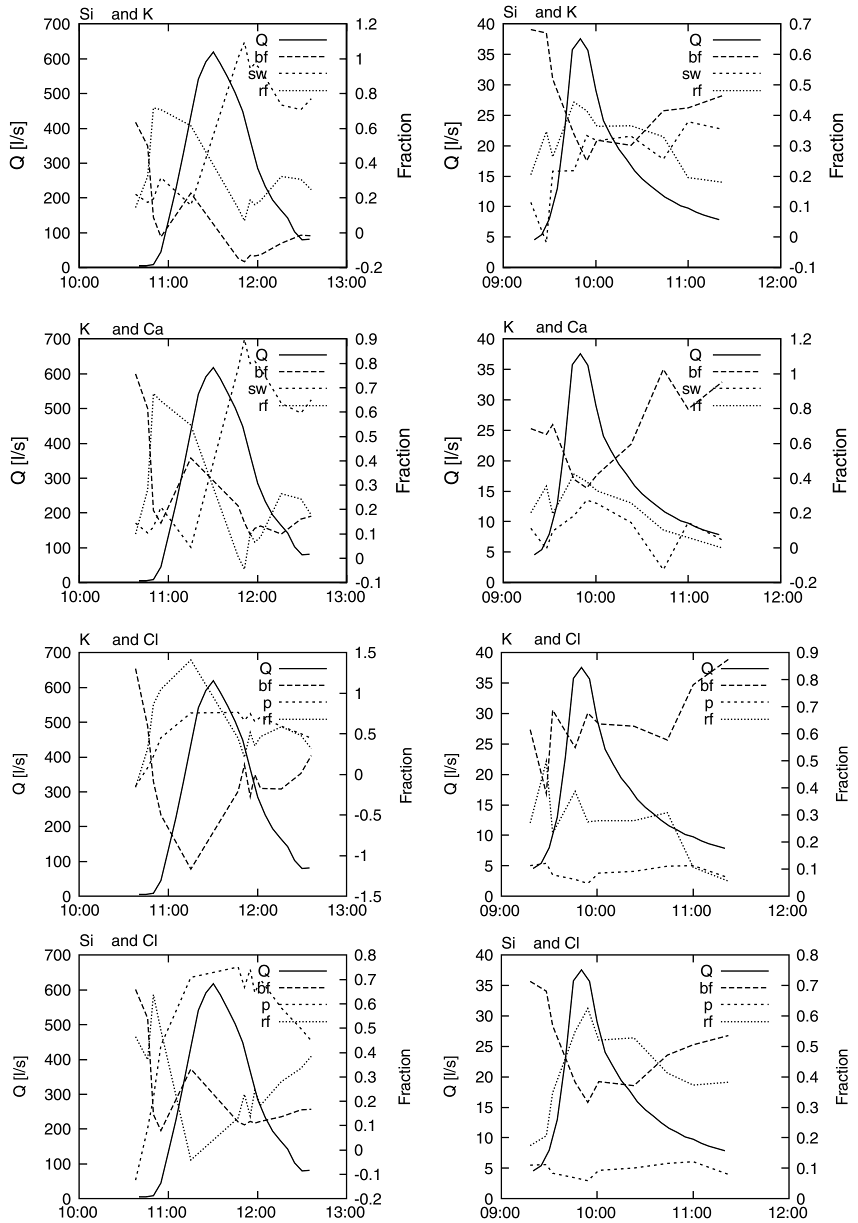


Figure 10. Discharge ($Q$, left-hand $y$-axes) and the fraction of total discharge (right-hand $y$-axes) contributed by the different flow components as established with a three-component mass-balance model for different hydrochemical constituent pairs during two storm events of contrasting magnitude at Bisley. The results for the large event are shown in the left-hand column and those for the small event are shown in the right-hand column

to 50 cm thick); (ii) a 5–40 m (depending on topographic position) layer of nutrient-poor highly weathered subsoil and saprolite material of medium to high resistivity; (iii) beneath this, a layer of low resistivity of 20–25 m thickness representing less-weathered saprolite material; (iv) a gradual change to unweathered bedrock (see also Figure 4). The zone of active weathering is located in the bottom part of layer (iii) at the contact with the bedrock. These results suggest that rock weathering at Bisley has proceeded for such a long

 

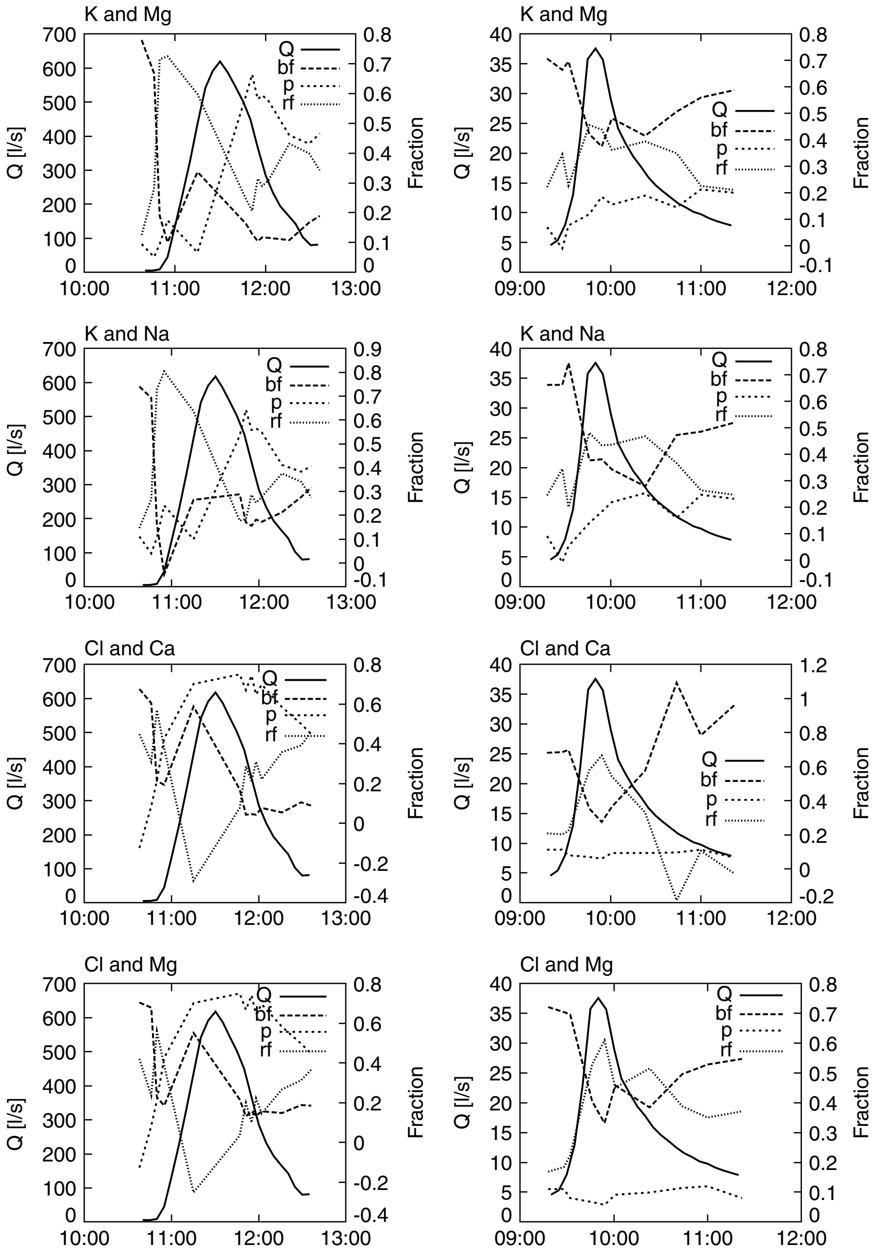


Figure 11. Discharge ($Q$, left-hand $y$-axes) and the fraction of total discharge (right-hand $y$-axes) contributed by the different flow components as established with a three-component mass-balance model for different hydrochemical constituent pairs during two storm events of contrasting magnitude at Bisley. The results for the large event are shown in the left-hand column and those for the small event are shown in the right-hand column

time that the weathering front, which is 60 m deep in places (Figure 4), has reached the local base level of the stream channel. The heavily leached nature of the saprolite (Figure 3B) and the available geological evidence suggesting that the Bisley area has been above sea level since Miocene times (Scatena, 1989) provide further support for this contention.

 

Table V. Average runoff component fractions as determined with a three-component mass-balance model for several constituent pairs for event I and event II at Bisley II

| Constituents | Large event ($P = 228$ mm) | | | | Small event ($P = 14{\cdot}3$ mm) | | | |
|---|---|---|---|---|---|---|---|---|
| | BF | SW | $P$ | RF | BF | SW | $P$ | RF |
| Si–K | 0·049 | 0·633 | | 0·318 | 0·439 | 0·250 | | 0·311 |
| K–Ca | 0·252 | 0·506 | | 0·243 | 0·658 | 0·112 | | 0·230 |
| K–Cl | −0·026 | | 0·496 | 0·529 | 0·641 | | 0·090 | 0·270 |
| Si–Cl | 0·215 | | 0·489 | 0·296 | 0·493 | | 0·094 | 0·412 |
| K–Mg | 0·244 | | 0·373 | 0·384 | 0·542 | | 0·135 | 0·323 |
| K–Na | 0·276 | | 0·358 | 0·366 | 0·493 | | 0·157 | 0·349 |
| Cl–Ca | 0·224 | | 0·489 | 0·288 | 0·646 | | 0·089 | 0·264 |
| Cl–Mg | 0·282 | | 0·487 | 0·231 | 0·528 | | 0·093 | 0·379 |
| Mean | 0·206 | | 0·449 | 0·349 | 0·557 | | 0·110 | 0·332 |
| Median | 0·234 | | 0·488 | 0·331 | 0·535 | | 0·094 | 0·335 |

The results of the saturated hydraulic conductivity ($K_{sat}$) measurements in auger holes show an apparent rapid decrease in $K_{sat}$ with depth. The results from the small core samples are less convincing, as the confidence limits for the depth zones overlap. Davis *et al*., (1996) demonstrated the importance of core sample size to the ultimately estimated $K_{sat}$ for soils with abundant macropores such as forest soils. Large core samples generally give much higher $K_{sat}$ values. This is illustrated further by the large difference in topsoil $K_{sat}$ values obtained with small core samples and the reversed auger hole method in the present study (Table I). The auger hole method covers a much larger sample that will include many more macropores, thus yielding much higher estimates for $K_{sat}$. The fact that the $K_{sat}$ estimates for the intermediate layer (20–50 cm) differed significantly less between methods suggests that macropores are becoming less important with depth (Table I). Similarly contrasting results were obtained by McDowell *et al*., (1992) in another part of the Bisley area, where a large difference was noted between topsoil $K_{sat}$ derived by infiltrometry (1–20 m day$^{-1}$) and values estimated for the deeper layers using well recovery tests (0·009–0·09 m day$^{-1}$). Figure 12 shows saturated conductivity profiles for the present study catchment and three other data-rich tropical forest sites. The La Cuenca catchment in western Amazonia experiences modest rainfall intensities but its $K_{sat}$ profile shows a sharp decrease with depth (Elsenbeer *et al*., 1992). As a result, widespread overland flow on hillslopes occurs frequently at this site. A similarly sharp decline in $K_{sat}$ with depth has been reported for the soils of the Babinda catchment in northeast Queensland, Australia (Bonell *et al*., 1981). Although the high $K_{sat}$ values of the topsoil at Babinda allow rapid subsurface stormflow, the combination of very high rainfall intensities and the presence of an impeding layer at shallow depth also result in widespread saturation overland flow (Bonell and Gilmour, 1978). The profile for the Bisley II catchment also shows a significant decline in $K_{sat}$ with depth, although this is less extreme than for the La Cuenca and Babinda catchments (Figure 12). Whether or not the partitioning of rainfall into subsurface stormflow and saturation overland flow demonstrated for Babinda and La Cuenca also occurs at Bisley cannot be decided conclusively in the current investigation. We suspect that subsurface stormflow is the prevailing mechanism for delivering rainfall into the stream channel.

*Response to precipitation*

Streamflow response to precipitation at Bisley is rapid, with less than 10 min delays, on average, between precipitation and discharge peaks (see Figure 6A). The small size of the catchment, the steep topography and the highly permeable topsoil with its abundant macropores are the most likely factors generating this rapid response. However, the nearly instantaneous response of the piezometers to precipitation (Figure 6B) must be regarded as anomalous, as it can be explained only by short-circuit flow through macropores. Further support for this contention comes from the remarkably high concentrations of potassium in shallow

 

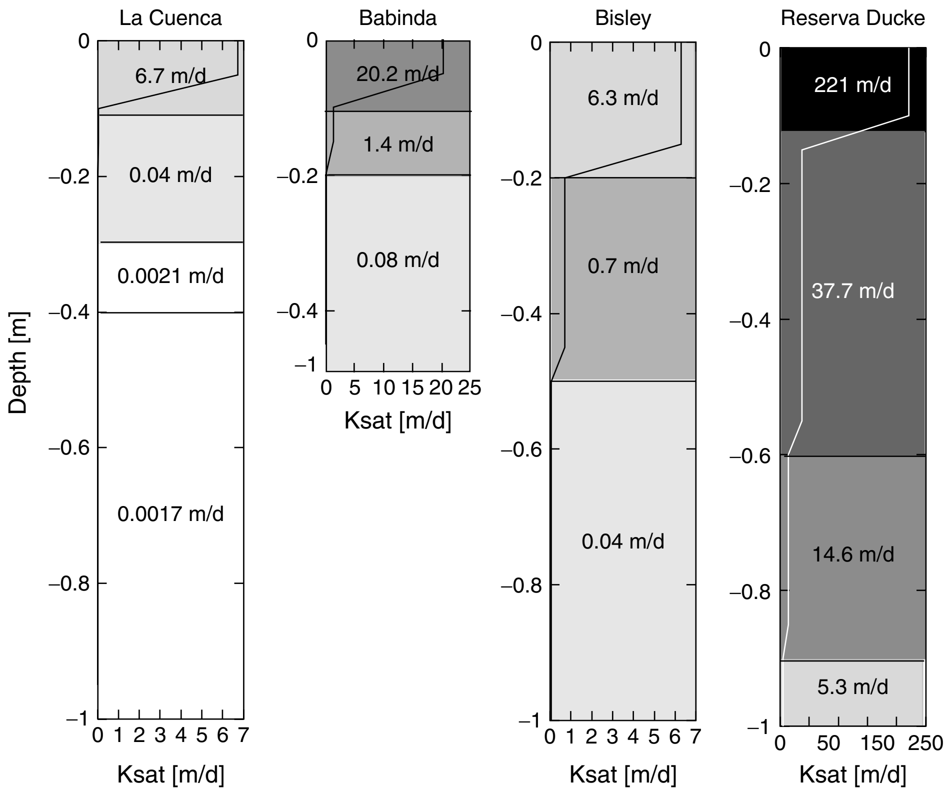


Figure 12. Schematic diagram comparing the changes in saturated hydraulic conductivity ($K_{sat}$) with depth for the study and three other tropical forest sites: La Cuenca, western Amazonia (Elsenbeer *et al*., 1992); Babinda, north east Queensland (Bonell *et al*., 1981) and central Amazonia (Nortcliff and Thornes, 1981)

groundwater samples (Table IV). Potassium is known to originate from near-surface sources, notably the litter layer (Waterloo, 1994; Elsenbeer *et al*., 1995a; Burghouts *et al*., 1998). Thus, the combined hydrometric (Figure 6B) and hydrochemical (Table IV) evidence suggests that the piezometers tapped water travelling through macropores in the upper part of the soil (*CF* McDowell *et al*., 1992). Larsen and Torres-Sanches (1990) had piezometers installed at similar topographic positions in the nearby Bisley III catchment, which showed a much slower response time that was more in line with measured $K_{sat}$ values. In their case, short screens were used that were sealed with bentonite at the top. This probably prevented the short-circuit flow that was encountered in the present study. Although the current piezometers did, therefore, not function as intended, the results do provide additional evidence for the occurrence of fast flow through the top part of the soil down to the riparian zone.

As shown in Figure 3C, the soil at Bisley becomes drier with depth below about 3·5 m, and no groundwater was found in any of the boreholes down to a depth of 8 m. Similarly, Larsen and Torres-Sanches (1990) reported gravimetric soil moisture profiles in the Bisley area to range from 37% at the top of the soil to 17% in the deeper (>1·6 m) layers. Additional support for the contention that relatively small volumes of water are actually percolating vertically to the deeper subsoil, with lateral pulses though the topsoil being both frequent and volumetrically more important, comes from the soil water modelling exercise. As shown in Figure 5, modelled soil water tensions at the ridgetop site were more frequently close to saturation than those deeper in the soil profile. If no allowance had been made for lateral drainage, the soil profile would have become saturated very rapidly and the soil water depletion curves (e.g. between 22 June and 7 July 1996) would have been much too slow (Figure 5). At 123 mm, the total volume of the inferred lateral flux between 5 May and 9

 

July 1996 far exceeded the 4 mm of water draining beyond a depth of 185 cm. Figure 6 and 7 illustrate two important aspects in this respect: (i) the hydrograph of the tributary gully closely resembles the amount of lateral drainage that is modelled for the top 10 cm of the soil profile (Figure 7A and B), whereas the timing of the peaks and the point at which the gully starts to hold water agree closely; (ii) the resemblance of the gully hydrograph to the stormflow hydrograph of the main stream channel can be taken as another indication of the importance of rapid subsurface stormflow in the study catchment (Figure 6A).

The combined data of Tables II and III provide a picture of a catchment whose response to rainfall is dominated by rapid flow paths. On average, an equivalent of 9% of the precipitation during storm events leaves the catchment as quickflow, with a maximum value of 28% (Table II). Taking the (very high) interception losses at Bisley (about 50%; Schellekens *et al*., 1999) into account, these values increase to 18% and 56% respectively. The correlation matrix linking stormflow parameters to potential causal variables in Table III shows that quickflow amounts (column 4) are highly correlated to rainfall parameters (notably for amount, less so for intensity) but hardly so to parameters describing antecedent wetness conditions, such as soil moisture and precipitation in the preceding days. These conclusions must be viewed with considerable caution, however, because the soil moisture data that were used in the analysis only represent a single element on a ridgetop, which can hardly be held representative for the entire catchment. Nevertheless, the results of Table III suggest that rainfall characteristics outweigh antecedent influences in this particular catchment.

*Water and soil chemistry*

The results presented in Table IV present a familiar picture: concentrations of hydrochemical constituents are lowest in precipitation and highest in stream water during baseflow (Bruijnzeel, 1983b; Waterloo, 1994; Elsenbeer *et al*., 1995a). However, some of the results deviate from the usual. For instance, calcium concentrations in soil moisture at Bisley were lower than in precipitation. This may be related to the limited number of precipitation samples ($n = 3$), but could also be caused by preferential uptake of calcium by the vegetation (Jordan, 1985). In addition, calcium concentrations in precipitation are likely to vary more in time than those in soil water. McDowell (1998) found a positive relation between storm size and calcium concentrations in throughfall in the nearby forest at El Verde. Adding this to the fact that soil water samples collected by vacuum tube lysimetry often 'integrate' the inputs from a number of storms, due to the time lag between precipitation infiltration and redistribution of soil water into the soil matrix, suggests that the apparently anomalous low concentrations of calcium in soil water may also be explained in terms of such temporal dynamics.

Because silicon concentrations are strongly governed by the contact time of the water with the soil they can be used to indicate the relative residence times of the respective water types (Bruijnzeel, 1983a). As such, baseflow can be expected to have the highest silicon concentrations. However, as none of the runoff sources that were sampled had silicon concentrations that resembled those of the baseflow (Table IV) it must be concluded that the actual source of the baseflow was not sampled. Working at nearby El Verde, McDowell (1998) also noted that concentrations during baseflow were considerably higher than any of the sources that were sampled. Brouwer (1996) reported enhanced elemental concentrations in matrix soil water flowing downslope along the contact between saprolite and fresh bedrock at a depth of 4 m in Guyana. A similar mechanism may be at work at Bisley. Based on the combination of geophysical and geochemical evidence, it may be assumed that some of the soil water percolates through the saprolite zone of low resistivity (Figure 3). The zone around the saprolite–bedrock contact may well be the source of the water having such high concentrations of silicon. On a related note, the stream base in the upper reaches of the catchment is closer to the zone of low resistivity (Figure 4), enhancing the chances for water coming into contact with the less-weathered parts of the substrate. This contention is strengthened by the results of an EC routing along the stream channel, which showed a steady increase in EC when going upstream (Van Hogezand, 1996).

 

*Chemical flow separation*

Elsenbeer *et al.* (1995b) highlighted some of the problems that may be encountered when trying to apply mixing models to catchments whose runoff response is dominated by fast flow paths, such as return flow and various forms of overland flow. The soil physical (Table I) and hydrometrical parts (Table IV, Figure 7) of the present study already suggest that the Bisley II catchment's response is also dominated by fast flow paths. Our mixing model application (Table V) provides additional evidence for this. However, some ambiguities remain. Looking at the respective constituent pairs used in Table V to separate contributions by baseflow, precipitation and return flow, the importance of the fast flow paths (especially during the large event) is evident (see also the bottom two rows of Figure 10 and all of Figure 11). On the other hand, when Si–K and K–Ca were used as constituent pairs, a very large contribution was calculated for soil water, especially at the end of the large event (Figure 10). Because soil matrix water cannot be regarded as a fast flow component, something else must cause this apparent anomaly. McDonnell (1990) described how rapid mixing of 'old' soil matrix water with fast-flowing 'new' water through macropores could explain a similar pattern in the steep Maimai catchment in New Zealand. Also, the sampling of soil water via tension lysimetry, as practised in the present study, makes the exact source of the water in the samplers (matrix or macropore water) uncertain (DeWalle *et al.*, 1988). However, it is pertinent in this respect that the computed 'soil water' contribution starts to increase only at the end of the large event, i.e. after a considerable amount of rain has fallen. Saturation overland flow (SOF) was not sampled directly in this study, although it was observed in the field (on a slope near the main stream channel) during the large storm and occasionally at other times. Combining this with the fact that the influence of the rainfall component (as shown in the top two rows of Figure 11) increases in a similar fashion as the apparent soil water contribution, it seems likely that SOF is the actual source at that moment, although only direct sampling will provide a more definite conclusion.

According to the mixing diagrams of Figure 9, it is clear that for some constituent pairs there is more than one choice of possible end member. For example, the bottom part of Figure 9 shows the ClMg and ClCa mixing plots for which BF, RF and P were chosen as end members. Instead of RF, SW could also have been chosen as, this would have included the whole mixing region as well. Figure 13 shows the result of doing so, with ClCa as the constituent pair. Combining these results with those of Figure 11, it appears that: (i) the large event (13 May 1996) is dominated by a different fast flow path than the smaller event; (ii) the 'real' soil water contribution to storm runoff (as apparent from Figure 13) is much smaller than envisaged originally in Figure 11 using RF as an end member; (iii) two fast flow paths, flow through macropores and SOF, emerge as the principal contributors to storm runoff in Bisley. However, the exact contribution of this SOF could not be determined, as it was not sampled directly, although it is clear that the large event includes a considerably bigger contribution by SOF than the smaller event (Figure 11).

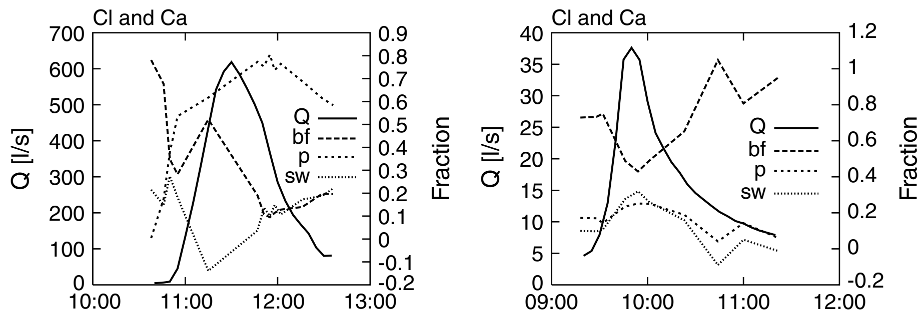


Figure 13. Discharge (left hand $y$-axes) and the fraction of total discharge (right hand $y$-axes) of the different flow components as established with a three-component mass-balance model using chloride and calcium with $p$, SW and BF as end members during two storm events of contrasting magnitude at Bisley. The large event is shown in the figure on the left and the small event is shown in the figure on the right

 

The present analysis used constant concentrations for the different sources. As noted by Hinton *et al*. (1994), this might be the greatest single source of error in predicted flow volumes, because the assumption of constant concentration is often not valid for many sources. Flushing effects (notably for potassium and calcium) are examples, especially during large events (see Figure 8).

### *A conceptual model of the runoff generation picture in the Bisley II catchment*

The present results suggest a picture of a catchment whose storm response is dominated by fast flow paths. The rapid decay of saturated hydraulic conductivity with depth (Table 1) clearly allows only small quantities of water to percolate to the deeper parts of the soil profile. The continuous decrease in soil moisture with depth below 3·5 m underlines this further (Figure 3C, *CF* Larsen and Torres-Sanches, 1990). The combination of the above and the topography in parts of the catchment favours rapid lateral flow through the uppermost soil horizon (subsurface storm flow, SSSF). The discrepancy between results obtained with different methods for the measuring of saturated hydraulic conductivity in the topsoil, in this and other studies in the Bisley area (McDowell *et al*., 1992), suggests that abundant macropores and a pronounced soil structure are the primary reasons for the relatively high conductivity of the topsoil (Table 1). Another source of rapid flow in the area is SOF. This type of flow is favoured by a rapidly decreasing hydraulic conductivity with depth, which allows a perched water table to develop easily, especially under high rainfall conditions (Bonell and Gilmour, 1978). At places where SSSF converges, such as in hillslope hollows, return flow (RF) may emerge, which again causes SOF, showing that the two flow types can be closely linked (Dunne, 1978, Elsenbeer and Cassel, 1990). The mixing model results presented in Figure 10 and 11 point to return flow (as measured in a tributary gully) as the main contributor to quick runoff. Additional hydrometric evidence (Figure 6) supports this contention. However, SOF (including precipitation onto already saturated areas) may also account for a significant portion of the quickflow at Bisley, especially during large events. Although the choice of end members and constituents used in the flow separation procedure influences the results considerably (*CF* Figures 10 and 11), it is clear that fast flow paths comprise an important part of the storm hydrograph at Bisley. Nevertheless, the baseflow percentage inferred for the smaller of the two sampled events is still considerable (56% on average, versus 20% for the large event). As discussed earlier, a flaw in the present application of the mixing model is the fact that we have not been able to sample the deep source of the baseflow directly. Two sources remain possible candidates: (i) soil water that flows along the weathering front before entering the stream channel; (ii) soil moisture (or even groundwater) from unsampled parts of the catchment, where either less weathering has occurred or the weathering zone is closer to the surface (e.g. due to tectonic activity). Further work is necessary, which could usefully employ stable isotope analytical techniques (Brammer and McDonnell, 1996, Nimz, 1998).

## ACKNOWLEDGEMENTS

The people at the hydrochemistry laboratory of the Faculty of Earth and Life Sciences of the Vrije Universiteit, Amsterdam, notably Mrs Hetty Schäfer, are thanked for processing the water samples. The assistance of the faculty's workshop and fieldwork equipment store is gratefully acknowledged. We further thank the electronics department of the faculty, notably J. de Lange and R. Lootens, for their help. The assistance of the chemical laboratory of the International Institute for Tropical Forestry, Rio Piedras, with the soil chemical analyses and F. Holwerda and A.J. Wickel in collecting core samples is gratefully acknowledged.

We gratefully acknowledge the efforts of the anonymous reviewers that allowed us to improve this paper significantly.

## REFERENCES

Beven K, Germann P. 1982. Macropores and water flow in soils. *Water Resources Research* **18**(5): 1311–1325.

Bonell M. 1993. Progress in the understanding of runoff generation dynamics in forests. *Journals of Hydrology* **150**: 217–275.

 

Bonell M, Fritsch JM. 1997. Combining hydrometric–hydrochemistry methods: a challenge for advancing runoff generation process research. In *Proceedings of the Rabat Symposium*; 165–184.

Bonell M, Gilmour DA. 1978. The development of overland flow in a tropical rainforest catchment. *Journal of Hydrology* **39**: 365–382.

Bonell M, Gilmour DA, Sinclair DF. 1981. Soil hydraulic properties and their effect on surface and subsurface water transfer in a tropical rainforest catchment. *Hydrological Sciences of Bulletin* **26**: 1–18.

Brammer DD, McDonnell JJ. 1996. An evolving perceptual model of hillslope flow at the Maimai catchment. In *Advances in Hillslope Processes*, Anderson MG, Brooks SM (eds). Wiley: Chichester, 35–60.

Brouwer LC. 1996. *Nutrient cycling in pristine and logged tropical rain forest*. Tropenbos Guyana Series 1. Georgetown, Guyana.

Brown S, Lugo AE, Silander S, Liegel L. 1983. *Research history and opportunities in the Luquillo Experimental Forest*. General Technical Report SO-44. USDA Forest Service, Southern Forest Experiment Station, New Orleans, LA, USA.

Bruijnzeel LA. 1983a. Evaluation of runoff sources in a forested basin in a wet monsoonal environment: a combined hydrological and hydrochemical approach. In *Hydrology of Human Tropical Regions*, Keller R (ed.). IAHS Publication no. 140. IAHS Press: Wallingford; 165–174.

Bruijnzeel LA. 1983b. *Hydrological and biochemical aspects of man-made forests in south-central Java, Indonesia*. PhD thesis, Faculty of Earth Sciences, Vrije Universiteit, Amsterdam.

Bruijnzeel LA. 1990. *Hydrology of Moist Tropical Forests and Effects of Conversion: A State-of Knowledge Review*. Unesco International Hydrological Programme: Paris.

Bruijnzeel LA. 1993. Land-use and hydrology in warm humid regions: where do we stand? In *Hydrology of Warm Humid Regions*, Gladwell JS (ed.). IAHS Publication no. 216. IAHS Press: Wallingford; 1–34.

Burghouts TBA, van Straalen NM, Bruijnzeel LA. 1998. Spatial heterogeneity of element and litter turnover in a Bornean rain forest. *Journal of Tropical Ecology* **14**: 477–506.

Chappell N. 1998. *Upscaling water, sediment flows in disturbed rainforest mosaics to the lumped catchment unit*. Final report on NERC project gr3/9439, Institute of Environment & Natural Sciences, University of Lancaster, Lancaster, UK.

Davis SH, Vertessy RA, Dunkerley DL, Main RG. 1996. The influence of scale on the measurement of saturated conductivity in a forest soil. In *23rd Hydrology and Water Resources Symposium*, Hobart, Australia, 103–108.

DeWalle DR, Swistock BR, Sharpe WE. 1988. Three-component tracer model for stormflow on a small Appalachian forested catchment. *Journal of Hydrology* **104**: 301–310.

Dunne T. 1978. Field studies of hillslope flow processes. In *Hillslope Hydrology*, Kirkby MJ (ed.). Wiley: 227–293.

Edmisten J. 1970. Soil studies in the El Verde rain forest. In *A Tropical Rain Forest*, Odum HT, Pidgeon RF (eds). US Atomic Energy Commission: chapter H-3, H-79–H-86.

Elsenbeer H, Cassel DK. 1990. Surficial processes in the rainforest of western Amazonia. In *Research Needs and Applications to Reduce Erosion and Sedimentation in Tropical Steeplands*, Ziemer RR, U'Loughlon CL, Hamilton LS (eds). IAHS Publication no. 192. IAHS Press: Wallingford; 289–297.

Elsenbeer H, Lack A. 1996. Hydrometric and hydrochemical evidence for fast flowpaths at La Cuenca, western Amazonia. *Journal of Hydrology* **180**: 237–250.

Elsenbeer H, Cassel K, Castro J. 1992. Spatial analysis of soil hydraulic conductivity in a tropical rain forest catchment. *Water Resources Research* **28**(12): 3201–3214.

Elsenbeer H, Lack A, Cassel K. 1995a. Chemical fingerprints of hydrological compartments and flowpaths at La Cuenca, western Amazonia. *Water Resources Research* **31**(12): 3051–3058.

Elsenbeer H, Lorieri D, Bonell M. 1995b. Mixing model approaches to estimate storm flow sources in an overland flow-dominated tropical rain forest catchment. *Water Resources Research* **31**(9): 2267–2278.

García-Martinó AR, Scatena FN, Warner GS, Civo DL. 1996. Statistical low flow estimations using GIS analysis in humid montane regions in Puerto Rico. *Water Resources Bulletin* **32**(6): 1259–1271.

Genereux DP, Hemond HF, Mulholland PJ. 1993. Use of radon-222 and calcium as tracers in a three-end-member mixing model for streamflow generation on the West Fork of Walker Branch Watershed. *Journal of Hydrology* **142**: 167–211.

Gosh DP. 1971. The application of linear filter theory to the direct interpretation of geoelectrical resistivity sounding measurements. *Geophysical Prospecting* **19**: 192–217.

Hewlett JD, Hibbert AR. 1967. Factors affecting the response of small watersheds to precipitation in humid areas. In *Forest Hydrology*, Sopper WE, Lull HW (eds). Pergamon Press: 275–290.

Hinton MJ, Schiff SL, English MC. 1994. Examining the contributions of glacial till water to storm runoff using two- and three-component hydrograph separations. *Water Resources Research* **30**(4): 983–993.

Holwerda F. 1997. *A study of evaporation from lowland and montane tropical rain forests in the Luquillo Mountains, Puerto Rico*. Working Paper 3. Faculty of Earth Sciences, Vrije Universiteit. Amsterdam, The Netherlands.

Horton RE. 1933. The role of infiltration in the hydrological cycle. *Transactions, American Geophysical Union* **14**: 446–460.

Jepma CJ. 1995. *Tropical Deforestation A Socio-Economic Approach*. Earthscan Publications: London.

Jones JAA. 1971. Soil piping and stream channel initiation. *Water Resources Research* **7**: 602–610.

Jordan CF. 1985. *Nutrient Cycling in Tropical Forest Ecosystems*. Wiley: New York.

Kendall C, McDonnell JJ. 1993. Effect of intrastorm isotopic heterogeneities of rainfall, soil water and groundwater on runoff modeling. In *Tracers in Hydrology*, Peters NE, Hoelm E, Lerbundgut Ch, Tase N, Walling DE (eds). IAHS Publication no. 215. IAHS Press: Wallingford; 41–48.

Kessler J, Oosterbaan RJ. 1973. *Determining hydraulic conductivity of soils*. In I.L.R.I. Publication no. 16. Volume III. International Institute for Land Reclamation and Improvement: Wageningen, The Netherlands, 253–296.

Koefoed O. 1979. *Geosounding Principles, 1: Resistivity Sounding Measurements*. Methods in Geochemistry and Geophysics, Vol. 14a. Elsevier: Amsterdam.

Lal R. 1987. *Tropical Ecology and Physical Edaphology*. Wiley: Chichester, UK.


 

Larsen MC, Torres-Sanches AJ. 1990. Rainfall soil moisture relations in landslide-prone areas of a tropical rain forest, Puerto Rico. *Tropical Hydrology and Caribbean Water Resources*: **July**: 121–129.

Lewis LA. 1974. Slow movement of earth under tropical rain forest conditions. *Geology* **2**: 9–10.

Lewis LA. 1976. Slow soil movement in the tropics—a general model. *Zeitschrift für Geomorphologie, Neue Folge, Supplementband* **25**: 125–144.

Lloyd CR, Marques-Filho A. 1988. Spatial variability of throughfall and stemflow measurements in Amazonian rain forest. *Agricultural Forest Meteorology* **42**: 63–73.

Loague K, Kyriakidis PC. 1997. Spatial and temporal variability in the R-5 infiltration data set: deja vu and rainfall-runoff simulations. *Water Resources Research* **33**: 2883–2895.

Lugo AE, Scatena FN. 1995. Ecosystem-level properties of the Luquillo Experimental Forest with emphasis on the Tabonuco forest. In *Tropical Forests: Management and Ecology*, Lugo AE, Lowe C (eds). Ecological Studies, Vol. 112. Springer-Verlag: New York, 59–108.

Marquardt DW. 1963. An algorithm for least-square estimates of nonlinear parameters. *Journal of the Society of Industrial and Applied Mathematics* **11**: 431–441.

McDonnell JJ. 1990. A rationale for old water discharge through macropores in a steep, humid catchment. *Water Resources Research* **26**(11): 2821–2832.

McDowell WH. 1998. Internal nutrient fluxes in a Puerto Rican rain forest. *Journal of Tropical Ecology* **14**(4): 521–536.

McDowell WH, Bowden WH, Asbury CE. 1992. Riparian nitrogen dynamics in two geomorphologically distinct tropical rain forest watersheds: subsurface solute patterns. *Biochemistry* **18**: 53–75.

Merz B, Plate EJ. 1997. An analysis of the effects of spatial variability of soil and soil moisture on runoff. *Water Resources Research* **33**: 2909–2922.

Molicova H, Grimaldi M, Bonell M, Hubert P. 1997. Using TOPMODEL towards identifying and modelling the hydrological patterns within a headwater, humid tropical catchment. *Hydrological Processes* **11**: 1169–1196.

Mosley MP. 1979. Streamflow generation in a forested watershed, New Zealand. *Water Resources Research* **15**(4): 795–806.

Mosley MP. 1982. Subsurface flow velocities through selected forest soils, South Island, New Zealand. *Journal of Hydrology* **55**: 65–92.

Mualem Y. 1976. A new model for predicting the hydraulic conductivity of unsaturated porous media. *Water Resources Research* **12**(3): 513–522.

Nepstad D, Verissimo A Alencar A, Nobre C, Lima E, Lefebvre P, Schlesinger P, Potter C, Moutinho P, Mendoza E, Cochrane M, Brooks V. 1999. Large-scale impoverishment of Amazonian forests by logging and fire. *Nature* **398**: 505–508.

Nimz GJ. 1998. Lithogenic and cosmogenic tracers in catchment hydrology. In *Isotope Tracers in Catchment Hydrology*, Kendall C, McDonnell JJ (eds). Elsevier: Amsterdam, 247–289.

Nortcliff S, Thornes JB. 1981. Seasonal variations in the hydrology of a small forested catchment near Manaus, Amazonas, and the implications for its management. In *Tropical Agricultural Hydrology*, Lal R, Russel EW (eds). Wiley: Chichester, 37–57.

Odum HT, Abbot W, Selander RK, Golley FB, Wilson RF. 1970. Estimates of chlorophyll and biomass of the Tabonuco forest of Puerto Rico. In *A Tropical Rain Forest*, Odum HT, Pidgeon RF (eds). U.S. Atomic Energy Commission: Washington, DC, 3–I19.

Rose CW, Yu BF. 1998. Dynamic process modelling of hydrology and erosion. In *Soil Erosion at Multiple Scales*, Penning de Vries FWT, Agus F, Kerr J (eds). CABI: Wallingford, U.K., 269–286.

Scatena FN. 1989. *An introduction to the physiography and history of the Bisley Experimental Watersheds in the Luquillo Mountains of Puerto Rico*. General Technical Report SO-72. USDA, Forest Service, Southern Forest Experiment Station, New Orleans, USA.

Scatena FN. 1990a. Culvert flow in small drainages in montane tropical forests: observations from the Luquillo Experimental Forest of Puerto Rico. *Tropical Hydrology and Caribbean Water Resources*: July 237–245.

Scatena FN. 1990b. Watershed scale rainfall interception on two forested watersheds in the Luquillo mountains of Puerto Rico. *Journal of Hydrology* **113**: 89–102.

Scatena FN, Larsen MC. 1991. Physical aspects of hurricane Hugo in Puerto Rico. *Biotropica* **23**(4): 317–323.

Scatena FN, Silver W, Siccama T, Johnson A, Sanchez MJ. 1993. Biomass and nutrient content of the Bisley Experimental Watersheds, Luquillo Experimental Forests, Puerto Rico, before and after hurricane Hugo. *Biotropica* **25**(1): 15–27.

Scatena FN, Moya S, Estrada C, Chinea JD. 1996. The first five years in the reorganization of above-ground biomass and nutrient use following hurricane Hugo in the Bisley Experimental Watersheds, Luquillo Experimental Forest, Puerto Rico. *Biotropica* **28**(4a): 424–440.

Schellekens J. 1997. Vamps, a Vegetation–AtMosPhere–Soil water model. Faculty of Earth Sciences, Vrije Universiteit, 0·99 alpha edition.

Schellekens J, Scatena FN, Bruijnzeel LA, Wickel AJ. 1999. Modelling rainfall interception by a lowland maritime tropical rain forest in northeastern Puerto Rico. *Journal of Hydrology* **225**: 168–184.

Schellekens J, Bruijnzeel LA, Scatena FN, Bink NJ, Holwerda F. 2000. Evaporation from a tropical rain forest, Luquillo Experimental Forest, Puerto Rico. *Water Resources Research* **36**(8): 2183–2196.

Silver WL, Scatena FN, Johnson AH, Siccama TG, Sanchez MJ. 1994. Nutrient availability in a montane wet tropical forest: spatial patterns and methodological considerations. *Plant and Soil* **164**: 129–145.

Simon A, Larsen MC, Hupp CR. 1990. The role of soil processes in determining mechanisms of slope failure and hillslope development in a humid-tropical forest, eastern Puerto Rico. *Geomorphology* **3**: 263–286.

Smith RE, Hebbert RHB. 1979. A Monte Carlo analysis of the hydrologic effects of spatial variability of infiltration. *Water Resources Research* **15**: 419–429.

Stakman WP. 1973. Measuring soil moisture. In *I.L.R.I. Publication no. 16. Volume III*. International Institute for Land Reclamation and Improvement: Wageningen, The Netherlands, 221–251.

Telford WM, Geldart LP, Sheriff RE, Keys DA. 1976. *Applied Geophysics*. Cambridge University Press.

Turvey ND. 1974. *Nutrient cycling under tropical rain forest in central papua*. Occasional Paper 10. Department of Geography, University of Papua New Guinea, Port Moresby.

Van Beers WFJ. 1979. *The auger hole method*. Technical report International Institute for Land Reclamation and Improvement/ILRI, Wageningen, The Netherlands.

 

Van Dijk AIJM, Schellekens J, Groen MMA. 1997. *Geophysical survey of the Bisley I and II catchments, Luquillo Experimental Forest, Puerto Rico*. Working Paper 4. Faculty of Earth Sciences, Vrije Universiteit.

Van Genuchten MT. 1980. A closed-form equation for predicting the hydraulic conductivity of unsaturated soils. *Soil Science Society of American Journal* **44**: 892–898.

Van Hogezand RJP. 1996. *The use of chemical tracers in identifying stormflow generating processes in a small catchment in the Luquillo Mountains, Puerto Rico*. Hydrological modelling in a humid tropical island setting: with special reference to the Luquillo Experimental Forest, Puerto Rico, Working Paper 1. Faculty of Earth Sciences, Vrije Universiteit, Amsterdam, The Netherlands.

Vertessy RA, Elsenbeer H. 1999. Distributed modelling of storm flow generation in an Amazonian rainforest catchment: effects of model parameterization. *Water Resources Research* **35**(7): 2173–2187.

Waterloo MJ 1994. *Water, nutrient dynamics of Pinus caribaea plantation forest on former grassland soils in southwest Viti Levu, Fiji*. PhD thesis, Faculty of Earth Sciences, Vrije Universiteit, Amsterdam, The Netherlands.

Whipkey RZ. 1965. Sub-surface stormflow from forested slopes. *Bulletin of the International Association of Scientific Hydrology* **10**: 74–85.

Wit KE. 1962. *Meting van de doorlatendheid in ongeroerde monsters*. Rapport 17. ICW, Wageningen.

 